Technical Sciences
Academy of Romania
www.jesi.astr.ro

Journal of Engineering Sciences and Innovation
Volume 10, Issue 1 / 2025, pp. 55 - 92

C. Chemical Engineering, Materials Science and Engineering

Received ***20 September 2024*** *Accepted* ***10 March 2025***
Received in revised form ***27 January 2025***

Copper coatings of polymer matrix composites. A review.

FERARU MIHAELA (ILIE)[1], SIMONA - NICOLETA MAZURCHEVICI[1], TEODOR - DANIEL MÎNDRU[1], CONSTANTIN CARAUSU[1], DUMITRU NEDELCU[1,2*]

[1] *"Gheorghe Asachi" Technical University of Iasi, Blvd. Mangeron No. 59A, 700050, Iasi, Romania*
[2] *Technical Sciences Academy of Romania*

Abstract. Polymers in general have low tensile strength and modulus of elasticity, poor electrical conductivity, low thermal and erosion resistance and high sensitivity to ultraviolet (UV) radiation. A technique called polymer metallization (PM), whereby a metallic layer is deposited on the surface of polymer parts, mitigates these shortcomings and extends the applicability of polymers. There are various ways to metallise polymer surfaces. The most efficient ones are thermal spraying (TS), electroplating, chemical vapour deposition (CVD), and physical vapour deposition (PVD). The benefits of each of these approaches are listed below: The application range of PVD and CVD is constrained by workpiece size, shape, and productivity, and both processes entail significant equipment and processing expenses. Electroplating is limited by low adhesive strength and long production cycle, strongly linked to environmental risks/costs. The CVD method takes too long and wet processing conditions limit the range of possible applications. TS methods provide the highest deposition rate and are cheaper, greener and easier to implement in industry than other deposition methods. Of the TS methods, Cold Spray (CS) uses the lowest operational jet temperatures, does not pre-melt the metal particles for deposition, and limits the risks of metal powder oxidation and thermal damage to the substrate. Metals, alloys, polymers, ceramics, and composites can all be deposited with this method on a range of substrate materials. Other names for CS include supersonic particle deposition, kinetic sputtering, dynamic or kinetic metallisation, CS additive manufacturing (CSAM), and dynamic cold gas sputtering. The paper firstly presents a comparison between the main processing methods, after which different experimental results on the resulting microstructure, different mechanical and thermal properties of the copper-coated polymer composites are presented. All the aspects presented above are important from the point of view of the recommendations that can be made for the use of these copper-coated composites in different industrial fields.

[*]Correspondence address: dumitru.nedelcu@academic.tuiasi.ro

Keywords: polymer composites, copper, coatings, mechanical properties, thermal properties.

1. Introduction

The global polymer market reached $650 billion in 2020 and is on track to grow by 5% annually over the next five years [1]. Over the last two decades, polymers have become increasingly used in lightweight components due to their low density, simple processing, processability and weldability [2]. Component weight reduction is a requirement of the automotive, aviation and aerospace industries [3]. Typical polymers have low tensile strength and modulus of elasticity, poor electrical conductivity (EC), low thermal and erosion resistance, and high sensitivity to ultraviolet (UV) radiation [4]. A technique called polymer metallization (PM), in which a metallic layer is formed on the surface of polymeric parts, mitigates these shortcomings and extends the applicability of polymers.

Polymer surfaces are metallized by several methods. Among the most promising ones are physical vapor deposition (PVD), chemical vapor deposition (CVD) [5, 6], electroplating [7, 8] and thermal spraying (TS) [9, 10, 11]. PVD and CVD involve high equipment and processing costs and are limited in terms of productivity, workpiece size and shape. Electroplating is limited by low adhesive strength and high production cycle; it has a harmful influence on the environment. CVD takes too long and wet processing conditions limit the range of possible applications. TS methods provide a high deposition rate and are cheaper, greener and easier to implement in industry than other deposition methods. However, most TS methods use a high temperature gas flow, which damages temperature sensitive substrates. Of the TS methods, cold spray (CS) uses the lowest operational jet temperatures, does not pre-melt the metal particles for deposition, and limits the risks of metal powder oxidation and substrate thermal damage. The CS process is an additive manufacturing technique used for manufacturing new parts, repairing structures and applying coatings by high-speed powder deposition. The solid metal powder is accelerated in a preheated gas stream and directed toward the target surface. When the jet hits the target, the metal projectiles plastically deform and adhere to the surface. This process can deposit layers of metals, alloys, polymers, ceramics and composites on a variety of substrate materials. CS is also known as dynamic cold gas sputtering, kinetic sputtering, CS additive manufacturing (CSAM), supersonic particle deposition and dynamic or kinetic metallization. Pioneering experiments at Cambridge University [12] in 2006 demonstrated the feasibility of PM by CS. Since then, nearly 50 research articles have presented results of CS trials on polymers, half of which have been published since 2018. Reviews on cold spraying before 2018 [10, 13-16] are scarce on polymers, while among recent reviews [17-22], only Raoelison et al. [22] devoted a short section to polymer substrates. Parmar and co-workers [23] reported on the materials science aspects of PM by CS.

2. Comparative study between thermal spraying and cold spraying

2.1. Thermal spraying

The term thermal spraying (TS) encompasses several methods by which a jet of molten metal particles is directed onto a solid surface TS methods use either electrical, chemical, or kinetic energy to atomize the coating layer. Some TS methods convert different forms of energy to heat and accelerate the metal powder in different proportions prior to deposition. The range of carrier medium temperatures and powder spray speeds specific to each TS method is shown in Figure 1. Plasma spraying and electric arc spraying methods use electrical heating.
In plasma spraying, a jet of ionized gas generated using either direct current or radio-frequency current [24, 25] melts and directs the metal powder onto the target surface.
In electric arc sputtering method, an electric arc is created between the ends of two wires supplied with electric current; a pressurized air sends the metal droplets to the target surface, where they deposit and solidify forming the deposited layer, [26, 27].
Other spraying methods, such as high velocity oxy-fuel (HVOF) and hot spraying are based on the principle of chemical heating. In the flame spraying method, a powder or wire is melted and projected towards the substrate in a gas stream realized by burning propane, [31-33].

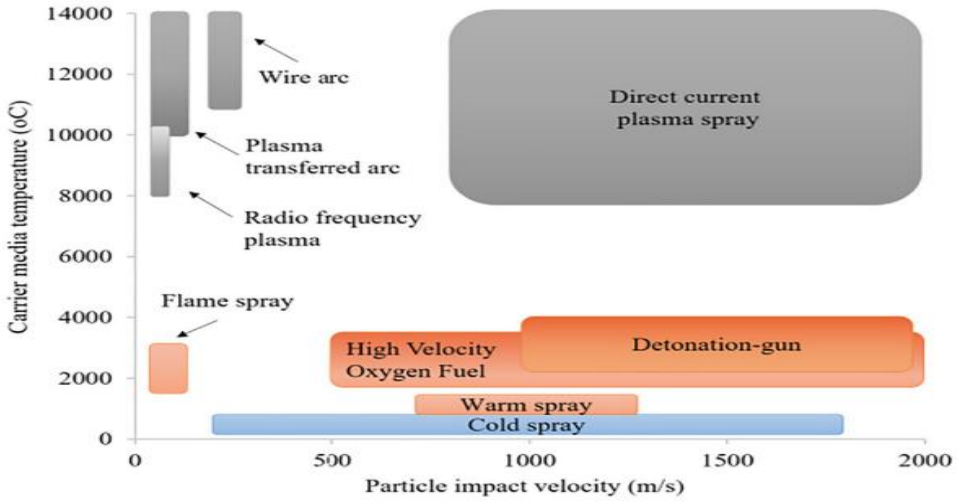

Fig. 1. Carrier medium temperature as a function of metal particle velocity in different thermal spraying methods. Colors indicate the type of energy input: gray - electrical; orange - chemical; blue - kinetic energy, [14, 28, 29, 30].

In HVOF, oxygen is mixed with a fuel, such as hydrogen, methane, propane, propylene or acetylene. The fuel-oxygen mixture is introduced into a combustion chamber, where it is ignited and burned continuously to propel the powder [34, 35]. The hot pulverization method is analogous to HVOF, but uses nitrogen instead of oxygen, which slightly decreases the temperature of the combustion gas [28].

Deposition by CS is achieved using the kinetic heating method [35]. In CS, the powder is accelerated to supersonic velocities by a pressurized hot gas, nitrogen or helium. Since the gas temperature range in CS (300-800) ◦C is insufficient for melting metal particles, gas preheating by using a convergent-divergent nozzle is used. The aerodynamic properties of the gas flow can be modified by altering the shape and dimensions of this nozzle [37, 38]. The gas momentum is transferred to the metal particles, which impinge on the substrate at supersonic velocity and undergo severe plastic deformation and melting, causing adiabatic shear instabilities and particle sticking [39]. The impact is assumed to remove oxide films, favoring contact between chemically clean particles and the substrate surface. In other words, the particles soften and become more adhesive by converting their kinetic energy into heat.

Thermal spraying has evolved over the last three decades, becoming a perspective method for depositing almost any material on any substrate, [40]. The term thermal sputtering encompasses a family of methods, in which metal powder is sprayed as a coating layer onto a solid surface [41]. The coating is formed by melting and deformation of the sputtered particles during sputtering or on impact. Figure 2 shows how the deposited layer is formed by sputtering of particles melted by heat from electrical, chemical or kinetic energy sources. All methods utilize a gun in which the deposition material is either melted or accelerated using an electric arc, flame, plasma or preheated gas and projected towards the target surface. The coating material is a metal, plastic or ceramic in the form of powder, wires or rods that are separated into particles within the spray and stick to the target surface on impact. When the target is completely covered by the impact particles, the particles that enter later stick to other particles and the coating is obtained.

Some SEM images of the coatings formed using different thermal spray methods are shown in Fig. 3, following particle image, top view and sectional view. In case A) flame spray, aluminum feedstock powder is used for coating and the coating was done on PU material. In case B) arc spray Zn particles in PE were used for coating and CFRP was used as coating material. In the case of plasma spray technology C), Cu splat on CFRP was used, and the coatings were Al on CFRP and Ti on PEEK. The last technology presented, cold spray (Figure 3), D), used Cu splatted on PVC, and the coatings were Cu on PEEK.

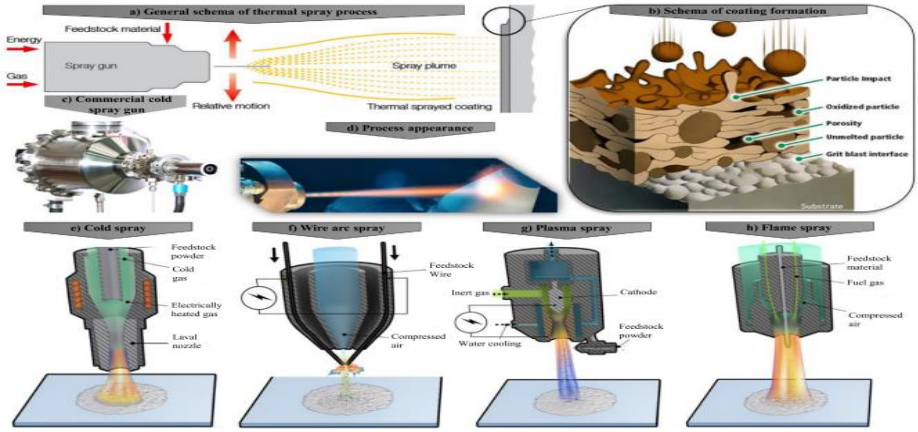

Fig. 2. Thermal spraying: a) process schematic; b) coating formation; c) commercial thermal spray gun; d) process appearance; e) cold spray; f) wire arc spray; g) plasma spray; h) flame spray, [40]

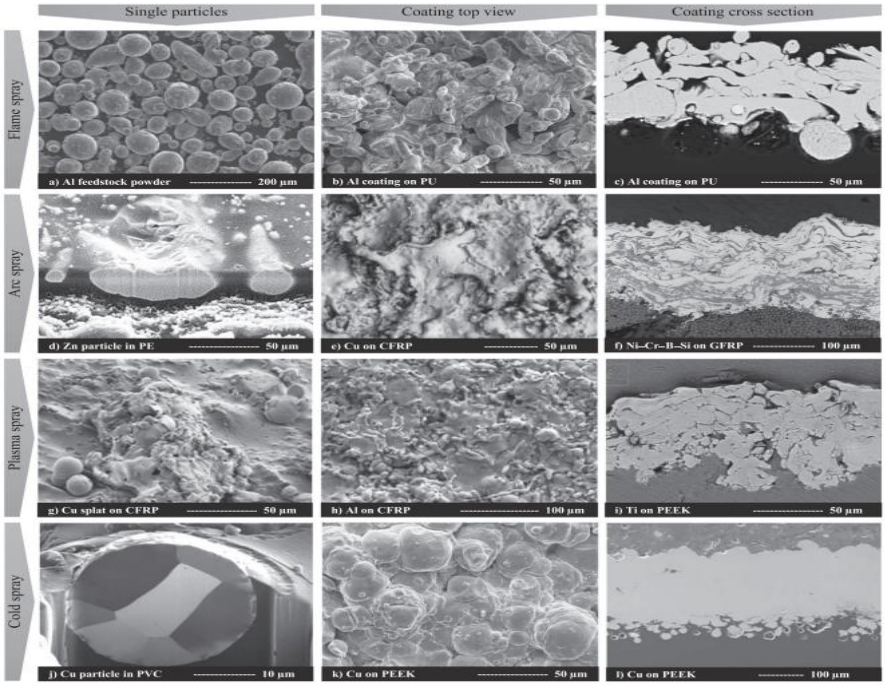

Fig. 3. SEM images of coatings formed by A) flame spray, [42]; B) arc spray, [42-45]; C) plasma spray, [42, 46-48]; D) cold spray, [49, 50]

2.2. Cold spraying

The deposition rate in CS is influenced by several factors, as follows: substrate material, surface condition, powders, gases used and process parameters, (Fig. 4).

The wide dispersion of the mechanical and thermal properties of polymers and composites leads to different reactions of polymers and composites to the particles with which the coating is made. Thus, due to the relatively low hardness, fatigue resistance, erosion resistance and high elasticity of the powder, only soft metal powder can be deposited directly on the polymer surface. Under these conditions, the main process parameters are gas temperature and pressure, which greatly affect the powder velocity, kinetic energy, strain rate and impact temperature. Secondary parameters are: surface nozzle away distance (SOD), gun travel speed and number of passes; these parameters can be used to tune the particle impact energy, deposition spot size and thermal softening of the substrate under the hot gas jet. These physical factors considerably influence various coating characteristics. The effects of the input parameters on the physical factors of the CS process and on the coating quality are discussed below, category by category.

Fig. 4. Classification of technological, physical and output factors of the cold spray process, [51]

2.2.1. Substrate material

CS coating of the substrate differs between polymers and steels. First of all, the glass transition temperature, i.e. the temperature at which a material loses its mechanical properties, is lower for thermoplastics than for metals. Second, the thermal conductivity is more than a hundred times lower in polymers than in metals, so that heat accumulates at the metal/polymer interface [52]. The deposition of the coating layer also depends on the plastic interaction between the particles and the substrate. On metal substrates, particle adhesion increases when the particles are substantially more plastic than the substrate. Most of the impact energy on polymeric substrates is consumed in the deformation of the substrate, which leads to particle embedding in the substrate [53]. Difficulties with polymer

coatings arise during subsequent build-up of the coating layer. Once a coating layer with embedded metal particles has formed on a polymer, subsequent impacts cause severe plastic deformation of both the coating layer and the impacted particles. Solid particle erosion frequently occurs at this stage. Subsequent impacts may destroy or damage the previously embedded layer if both impact particles are of the same material. A difference in hardness between the impact particles is needed so that some can absorb more impact energy and yield energy to the first particles.

Zhang et al., [29] were among the first to report the results of CS coatings on a polymer target; the effect of substrate hardness on Al powder deposition was examined using more than 10 metallic and ceramic substrates and an acrylonitrile butadiene styrene-butadiene acrylonitrile (ABS) substrate. Since ABS is a low-hardness substrate, all deformation occurred in the substrate, and not in the Al powder. The subsequent deposition of Al powder on ABS was clearly unsuccessful.

Che et al., [55] analyzed the particle impact spots on different polymers. Thus, Figure 5 shows the SEM images of a cold-sprayed Cu particle on each substrate. The images (a-d) were captured under the same conditions: gas at 425 ◦C impinging on the Cu particles at 530 m/s. Cu powder is very difficult to deposit on polymers because of its high melting point. However, Cu particles are softer than many metal substrates and therefore flatten easily during impact due to significant plastic deformation. This indicates that the particles have melted and recrystallized at the interface, allowing chemical adhesion through the metal bond. However, on the thermoplastic polymer substrates, the Cu particles did not flatten. PEEK and polyethyleneimine (PEI) substrates deformed significantly due to particle incorporation, while the particles themselves deformed insignificantly. In the softer ABS substrate, the particles were completely embedded. After several such deposits, a rigid anchored Cu layer is formed on the ABS surface. The first layer is not necessarily continuous but may show a sparse distribution of separated particles [55]. Such a layer does not guarantee further Cu accumulation.

Although they were unable to create a direct Cu layer on PVC, Ganesan et al. [56] were able to generate an anchoring Cu layer. The initial particles were firmly embedded and attached, as seen in the SEM images (Fig. 5e). However, later hits extruded the surrounding molten polymer, which remained as a film on top of the embedded particles (Fig. 5f). By serving as a separator between two Cu particles, this polymer film inhibits the formation of layers and their metallic connection. Multiple incorporation of Cu particles was achieved on ABS and PEEK, but a continuous layer was not subsequently built up [55]. The mass of some samples was slightly reduced after CS, indicating that the deposition was slightly compensated by erosion.

Che et al., [55] argued that metal coatings by CS should be considered as a two-step process: first layer formation and then accumulation. They suggested that each stage has its own technological "window" defined by lower and upper particle velocity thresholds, beyond which the particles are insufficiently melted for

bonding or start to erode the substrate, respectively. The substrates had hardnesses of 490, 110, 78 and 40 MPa, respectively [57].

2.2.2. Powder parameters

All materials selected for CS deposition have low melting point and low resistance to deformation. Metals that fulfill these properties are Sn, Cu, Zn, Ag, Bi, In and Al, together with their alloys and mixtures. Fe powders have also been cold sputtered successfully on various polymeric materials [55].

Gardon et al., [58] utilized process parameters by which Ti powder was bonded to PEEK, obtaining a 1 mm thick titanium layer. The coating layer had a homogeneous thickness and exhibited a well adherent, crack-free structure. Its content was the crystalline metallic Ti element. Unfortunately, the authors did not disclose the absolute values of the CS process parameters, but only their ratios, which do not allow reproducing the experiment. Typical powder materials used for metal coatings by means of CS are shown in Fig. 6.

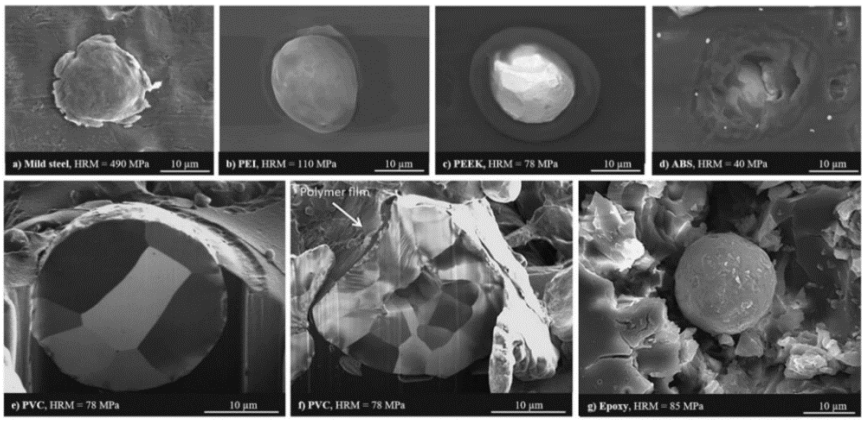

Fig. 5. Responses of different polymeric substrates to the impact of a spherical Cu particle with a diameter of 20 µm: a) mild steel; b) PEI; c) PEEK; d) ABS; e, f) PVC; g) Epoxy, [55, 57]

Lupoi and O'Neill [60] cold-sprayed 50-100 µm Cu, Al and Sn powders onto a range of plastics. They claimed that low density favored powder deposition by preventing or mitigating substrate erosion. The heavy particles result in high impact energy, creating severe contact stresses and consequently delamination of the coating interface. The pulverizing ability of a powder can be improved by premixing it with harder metallic or ceramic particles. The harder particles in the mixture increase the roughness of the substrate and improve particle interlocking. They also produce a microgrinding effect that compacts the underlying layers and reduces the porosity of the coating [61].

Physically, tamping can be accomplished using any particles (including metals) with hardness values exceeding that of the deposition powder. Some of these particles remain embedded in the substrate, forming a composite layer [62]. These composite microstructures (Fig. 7) can be beneficial in certain applications. For

example, the introduction of alumina improves the wear behavior and scratch resistance of Sn coating by up to 60% and 30%, respectively [63]. Cu and Al powders require high critical velocities for bonding during CS, they escalate substrate erosion during deposition. Erosion is the main obstacle against deposition of these materials on CFRP, [64].

To mitigate this phenomenon, Chu et al [64] mixed Sn powder with 10% of Cu, Zn or Al powder, thereby increasing the DE by 3-6 times. Thermodynamically, the enhancement of DE is due to the conversion of the kinetic energy of the secondary (hard) particles into strain energy and the heating of the already deposited primary (soft) particles. In this way, the second powdered additive facilitates the melting of the first one. However, the secondary particles are poorly deposited and most of them rebound from the surface. Che et al., [65] showed that the overall DE is inversely proportional to the percentage of Cu, Zn and Al dopant particles in the Sn powder. Combining Sn with a lower melting point powder, such as bismuth, allows deposition at a lower gas temperature compared to the temperature used for pure Sn powder.

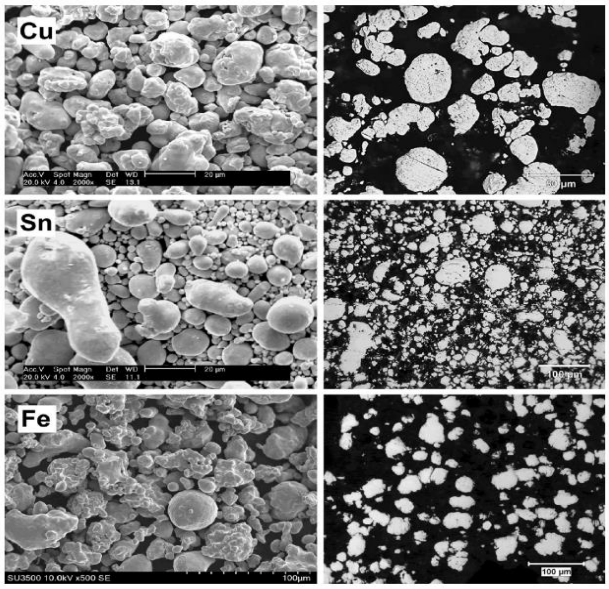

Fig. 6. SEM images (left) and cross-sectional optical micrographs (right) of raw material powders, [58, 59].

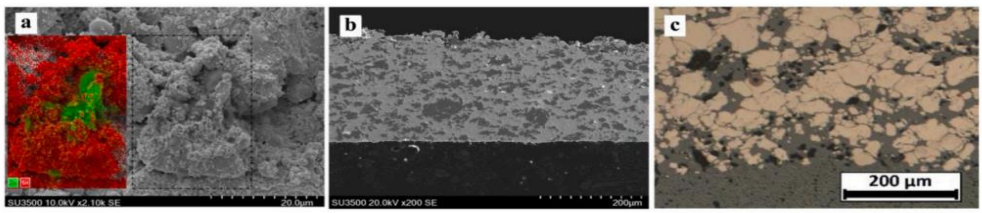

Fig. 7. Cold spray coatings: a) a Zn particle coated with Sn particles fused in CS with a Zn/Sn mixture (10/90 wt%) [65], b) deposited layer of Cu and Sn (50/50 wt%) [65], c) deposited layer comprising PEEK and Cu (80/20 wt%) [66].

Bortolussi et al [66] mixed Cu with polymer powder to form a conductive layer on CFRP. They showed that the secondary component of the deposition mixture (i.e., the polymer powder) can effectively bind the metal powder while maintaining the existence of a percolated network of metal particles to ensure the macroscopic conductivity of the coating. By choosing certain sputtering parameters, powders with specific shapes, sizes and flow ratios, diverse microstructures with unique electrical and bonding properties can be produced. Bortolussi's team further pursued gradient composite coatings using CS with multiple powder feeders. This technological solution could eventually be the way to realize coatings with multiple properties. Another effect of powder blending is the customized flowability of the particles. The nozzle clogged rapidly when Sn was pulverized at 325 ◦C [67], but after mixing Sn powder with 30% Cu, the nozzle did not clog at gas temperatures below 350 ◦C, presumably due to the fact that the Cu particles served as "nozzle sweepers" that cleaned the nozzle [65]. Mixing the soft metal powder with ceramic particles also prevents nozzle clogging [68].
The effects of particle hardness were recently studied by Rokni et al., [69]. During high-pressure CS (HPCS) on PEEK and PEI, the DE of pure Al powder with hardness HV = 160 MPa was 20 times higher than that of Al 7075 powder with hardness HV = 350 MPa, but on ABS, the DE was independent of particle hardness.
In scratch tests, the pure Al coating on PEEK, PEI and ABS failed at (7-12) MPa, while the Al 7075 alloy coating on PEEK and PEI failed at (17-27) MPa. Residual stresses can be reduced by heat treatment; heat-treated powders exhibit higher strain capacity and DE.

2.2.3. Cold spray process parameters

At the National Research Council of Canada in Boucherville, cold spray tests were carried out on a McGillNRC cold spray facility. The cold sprayability of metal powders on polymer substrates at a variety of particle velocities was examined using two different systems: a high-pressure system (PSC-800, Plasma Giken, Japan) and a low-pressure system (SST, CenterLine, Canada). It should be noted that there are a number of differences between the two pressure systems (e.g., nozzle geometry, powder injection mode, and thermocouple location). Nitrogen was selected as the carrier gas for both systems, and the three powders mentioned above were sprayed under different conditions, which are detailed in Table 1.
In order to prevent melting, Sna was cold sprayed at 200°C, nickel was cold sprayed at 200°C, copper at 425°C, and iron at both 200°C and 425°C. The CenterLine system's additional process parameters were essentially the same as those used in earlier studies that resulted in effective deposition [71]. Although the gun travel speed of 25 mm/s for the Plasma Giken system is quite slow, it was maintained at the same level for the CenterLine system to allow for a direct comparison. Before cold spraying, the powder feeder's actual feed rate was measured for each powder and set at 1 rpm.

Table 1. Cold spray process parameters, [71]

Powder	Temperature [°C]	Pressure, [MPa] (psi)	Standoff distance, [mm]	Gun travel speed, [mm· s^{-1}]	Feeding [g·min^{-1}]
Low-pressure CenterLine system					
Sn	200	(75-200) 0.5-1.4	18	25	10
Fc	200	(75-200) 0.5-1.4	18	25	16
Fc	425	(50-200) 0.3-1.4	18	25	16
Cu	425	(50-200) 0.3-1.4	18	25	11
High pressure Plasma Giken system					
Fc	200	2-4	40	25	16
Fc	425	2-4.9	40	25	17
Cu	425	2-4.9	40	25	19

A particle diagnostic device (DPV2000, Tecnar Automation, Canada) that illuminates particles in flight with a laser diode (7 W, k = 830 nm) was used to detect particle velocities under various situations [72]. The laser was trained on the "centre" of the stream, where the majority of the particles were found, and the striking distance was maintained at the values indicated in Table 1. A total of 300 particles were found for every measurement.

2.2.5. Deposition efficiency and microstructure

From Fig. 8 it can be seen that the copper deposition on the steel substrate started at a gas pressure of 1.0 MPa, which corresponds to a velocity of 225 m/s; then, the DE increased with increasing gas pressure/particle velocity. At gas pressures higher than 2.0 MPa, DE could not be measured because the deposited layer continued to fall off the substrate during cold spraying, indicating poor adhesion, probably due to the effects due to the increase in layer thickness.

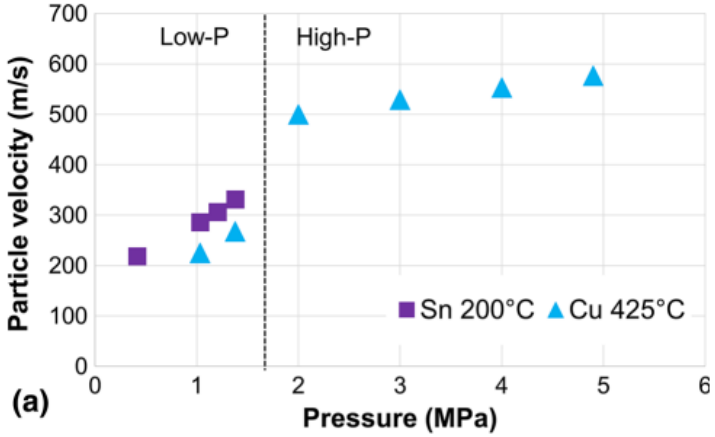

Fig. 8. Measured mean particle velocities as a function of gas pressure for Sn sputtered at 200°C and Cu sputtered at 425°C [72].

In the case of CFRP, significant erosion was similarly observed, although the material loss values were lower than for iron powder. Both PEEK and PEI materials displayed a trend of rising DE as gas pressure and particle velocity increased. At low pressures up to 1.4 MPa, they showed low DEs of 5%; however, at a lower gas pressure of 1.0 MPa, the DE of copper on steel began to climb dramatically. The DE on PEEK increased as a result of the high pressure system. This was similar to the DE at 2.0 MPa on the steel substrate, where the DE increased with increasing pressures and speeds. DE likewise increased significantly with respect to the PEI substrate beginning at 2.0 MPa; however, DE on PEI was less than that on the steel and PEEK substrates under the same circumstances. The peeling of the coating during the process prevented the DE measurement on PEI at 4MPa.

Figure 9 displays the DE results for cold sprayed copper at 425°C. The coating materials utilised were PEEK, ABS, PEI, CFRP, and steel. Figure 10 displays the micrographs obtained from cold spraying Cu at 425°C at gas pressures of 1.0 MPa (Figure 10 a, c) and 2.0 MPa (Figure 10 b, d).

Both ABS (Fig. 10a) and PEEK (Fig. 10c) showed significant embedding of the copper particles at the pressure at which deposition on the steel began, 1.0 MPa, but no continuous layer was created. It is evident that a substantial layer of copper was effectively deposited on PEEK when the gas pressure was raised to 2.0 MPa using a Giken Plasma system (Fig. 10d).

On the other hand, Fig. 10(b) depicts the deposition on ABS with a much lower number of embedded particles, compared to 1.0 MPa. This suggests that deterioration of the ABS substrate has happened, as does the somewhat negative DE value. With the Giken high-pressure plasma system, significant copper deposition can generally be achieved when cold-spraying at 425 °C on steel, PEEK, and PEI substrates.

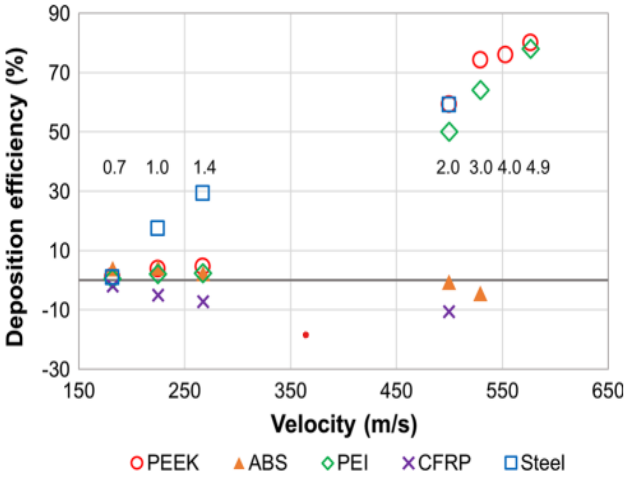

Fig. 9. Cold-sprayed Cu DE at 425°C on different substrates as a function of average particle velocity [73]

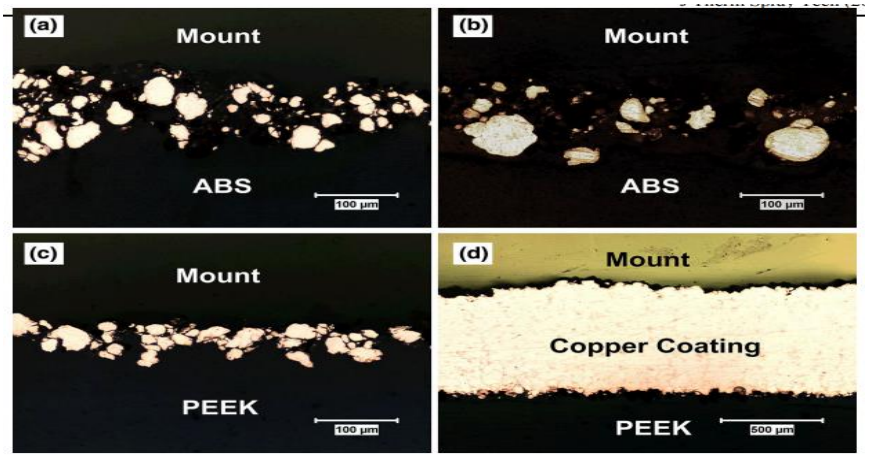

Fig. 10. Cross-sectional optical micrographs: a) ABS for 1MPa pressure; b) ABS for 2MPa pressure; c) PEEK for 1MPa pressure; d) PEEK for 2MPa pressure [74].

2.2.6. Substrate effect

Cold spraying of different metal powders on different substrates showed different results. For example, cold spraying of copper at 425°C at 2.0 MPa gas pressure was successful on PEEK, PEI and steel substrates, but failed on ABS and CFRP. The substrate may therefore play an important role in determining the cold sprayability of the metal powder. Researchers have reported that cold sprayability of metals on thermoplastic polymers is more successful than on thermoset polymers due to the local softening mechanism in thermoplastics [76, 77]. Significant substrate erosion was seen under various situations, and cold spraying on CFRP with thermoset matrix was determined to be unsatisfactory in most cases. More encouraging outcomes were seen for thermoplastics, where tin coatings and thick copper coatings were achieved on PEEK, thick copper coatings on PEI, and tin coatings on ABS. Similar findings reported by other researchers [76, 78] can be attributed to local softening of thermoplastics; that is, the polymer surface exposed to the gas/particle flow softens upon cold spraying at a temperature that approaches or exceeds the thermoplastic's Tg; metal particles then permeate the polymer and, upon cooling, mechanically lock with the polymer substrate. This technique allows the metal particles to penetrate the thermoplastic surface without undergoing significant plastic deformation, in contrast to typical splash formation [76]. This mechanism is characterised by waviness at the coating/substrate contact. Particle embedding and mechanical locking are relatively difficult at low impact velocities because the polymers are in a glassy state and are relatively hard and brittle at temperatures much lower than Tg. Local thermal softening is also difficult (e.g., failure in cold spray of tin at 200°C on PEI with glass transition temperature of 215°C), but at high impact velocities significant substrate erosion can occur due to brittleness. However, if the temperature is significantly greater than Tg, the thermoplastic's mechanical qualities may deteriorate significantly, deposition on the thermoplastic may be challenging, and substrate erosion may happen as a result

of the polymer strength deteriorating. The cold spraying of copper at 425°C onto ABS, whose Tg is 105°C, is an illustration of this.

When the copper particles hit the substrate's surface, their temperature can rise above 200°C, which can cause erosion and a serious decline in the ABS's strength. On the other hand, PEEK and PEI's success at 425°C can be attributed to their well-known capacity to preserve good mechanical qualities at comparatively high temperatures. For the purpose of cold spraying metals on polymer substrates, it is crucial to understand how temperature affects the characteristics of polymers. To completely comprehend the particle-substrate interaction during impact and, consequently, the mechanism of bond formation between the cold-sprayed particles and the polymer substrate, more research (such as single particle impact tests and numerical simulations) is required. During cold spraying, it is especially crucial to ascertain the substrate temperature as well as the temperature at which the particle and substrate interface meet.

Chaoyue Chena et al., [79], deposited Cu on the PEEK substrate using a cold sputtering system (LERMPS, UTBM, France), which is schematically depicted in Figure 11. The de-Laval type nozzle (MOC 24) was used, which has a circular cross section with an expansion ratio of 8.3. High pressure compressed air was used as powder carrier gas and propellant gas. The propellant gas at the nozzle inlet had a temperature of 300 °C. Different propellant gas pressures (1.2 MPa, 1.6 MPa, 2.0 MPa and 2.4 MPa) were used to investigate its influence on the metal coating on the PEEK substrate. The distance between the substrate and the nozzle outlet was set to 30 mm. The nozzle travel velocities for full and single particle deposition were set at 50 mm/s and 500 mm/s, respectively. The full Cu layer was achieved by 3 passes of the nozzle trajectory over the PEEK substrate. The spherical Cu powder which was produced by LERMPS (UTBM, France) with a gas atomization process.

The morphology of the Cu powder is shown in Fig. 12(a), and its size distribution, measured by laser diffraction particle size analyzer (Mastersizer 2000, MALVERN Instruments, UK), is shown in Fig. 12(b). The spherical Cu powder has an average diameter of 26.7 μm. The PEEK plates used as substrate have a size of (5 × 3)mm and are supplied by GEHR GmbH, [79].

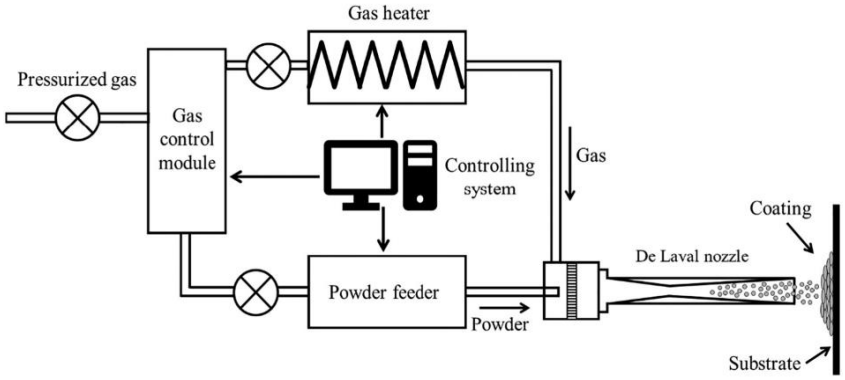

Fig. 11. Schematic diagram of the cold spraying process [79].

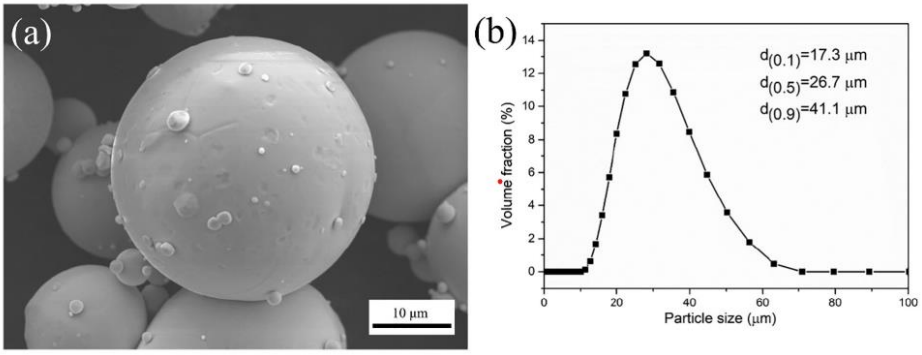

Fig. 12. Surface morphology (a) and size distribution (b) of Cu powder used [79].

The metallized substrates were also observed by scanning electron microscopy and characterized by EDX measurements. As shown in Fig. 13, in both cases, the metallic layer consists of nanoparticles with sizes ranging from 100nm to 200 nm, and the surface was not totally homogeneous on a microscopic scale; the metallic layer appears, however, to be more compact in the case of the copper plating bath. The plating bath and, especially, the metal growth are extremely difficult to control at laboratory scale. These plating baths are developed for an industrial production line. However, the section of ABS after Cu metallization showed a flat (Figure 13c) and homogeneous metallic top layer and a good interfacial area between the metal and ABS. After 10 min of coating the metal layer thickness is about (5-10)µm.

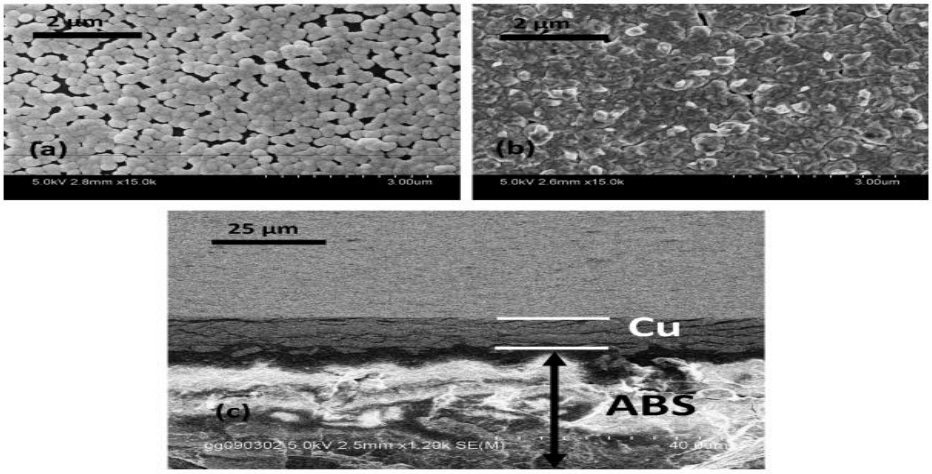

Fig. 13. SEM images after metal deposition without electrodeposition: (a) nickel and (b) copper plating with a top view at 2 µm scale and (c) copper plating with ABS section at 25 µm scale with a tilt angle of 75° [75].

Microstructure

Figure 14 shows the Cu layers sputtered on the PEEK substrate at different propellant gas pressures after 3 deposition passes. It can be seen that a dense and uniform Cu layer was produced on the PEEK substrate as the propellant gas pressure increased.

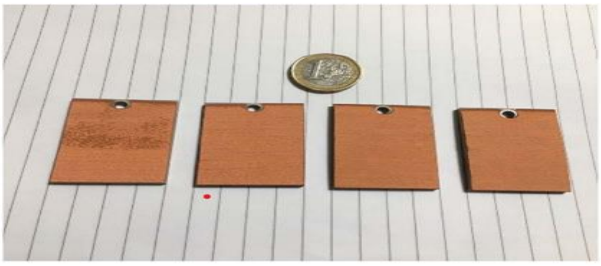

Fig. 14. Digital photographs of Cu layers sputtered on PEEK substrates after 3 deposition passes at different propellant gas pressures [81].

The cross-sectional morphology of the cold-sprayed Cu layer on the PEEK surface, realized at different propellant gas pressures, is shown in Fig.15. It can be seen that a thick and dense Cu layer was obtained on the PEEK surface. It can also be seen that the thickness of the coating layer increases with the increase in the propellant gas pressure.

The average thickness of the coating layer obtained at different propellant gas pressures is shown in Fig. 16. At a gas pressure of 2.4 MPa, the thickness of the Cu coating layer reached more than 400 μm in only three passes. One reason for this influence would be that with increasing gas pressure there is a higher plastic deformation of the particles, which directly results in a thicker deposited layer. Since the black areas in the coatings correspond to pores and microcracks, it can be seen that the porosity of the coating decreases with increasing gas pressure.

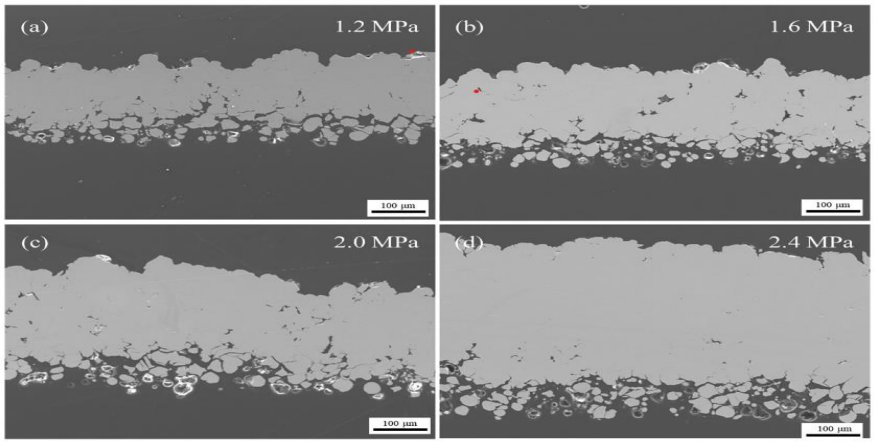

Fig. 15. Cross-sectional morphology of Cu coating on PEEK substrate at different propellant gas pressures: a) 1.2 MPa; b) 1.6 MPa; c) 2.0 MPa; d) 2.4 MPa, [82]

The variation of the porosity value of the Cu coating at different propellant gas pressures is shown in Figure 17. The coating layer porosity decreased below 1 % as the gas pressure is higher than 2.0 MPa, which can provide a desirable coating layer quality. Meanwhile, it should be noted that some micro-cracks between the deformed particles exist in the lower part of the coating near the PEEK substrate, while pores and cracks are fewer in the upper part of the coating. Due to the lack of sufficient hardness of the PEEK substrate, Cu particles cannot undergo sufficient plastic deformation. As reported by King [83], the binding mechanism between the Cu particle and various polymeric substrates is mainly a mechanical blockage that results in the impact particle trapping and penetration into the relatively soft polymeric substrate. Thus, the distinctive bonding mechanism in the metal/polymer deposition cannot avoid the porosity of the coating near the substrate. With successive successive particle impacts, the accumulation of the coating layer was realized by deposition between the deposited particles and the already formed layer. The successive peening effect and the strong plastic deformation of Cu particles on the PEEK layer resulted in a dense coating with low porosity. As the propellant gas pressure increases, this peening effect gradually intensifies, leading to a much lower porosity of the coating layer. Detailed discussion on the deposition mechanism of Cu layer on PEEK substrate will be carried out in the following sections.

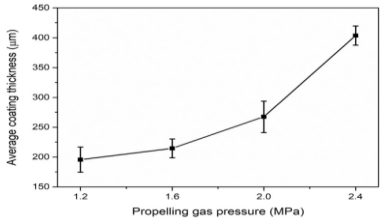

Fig. 16. Cu coating thickness as a function of propellant gas pressures [84].

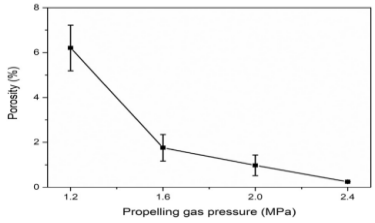

Fig. 17. Porosity of Cu coating as a function of propellant gas pressure [85].

Subsequently, the Cu particles that are at the next passes directly hit the first layer that is already formed on the PEEK substrate. The coating process has turned into metal-to-metal bonding rather than metal-to-polymer bonding. However, the quality of the coating layer is not so good for the area around the Cu/PEEK interface. An enlarged view of the interface between the layer and the substrate is shown in Figure 18. The PEEK substrate softened significantly upon impact with the high-velocity particle. Such a successful mechanical bonding can realize the deposition of the first Cu layer, which acts as a metallic substrate for the subsequent formation of a completely dense and thick Cu layer on the PEEK surface. In addition, it has been reported that the PEEK structure can be modified or destroyed upon severe plastic deformation [86], which can potentially affect the deposition realization on the PEEK material.

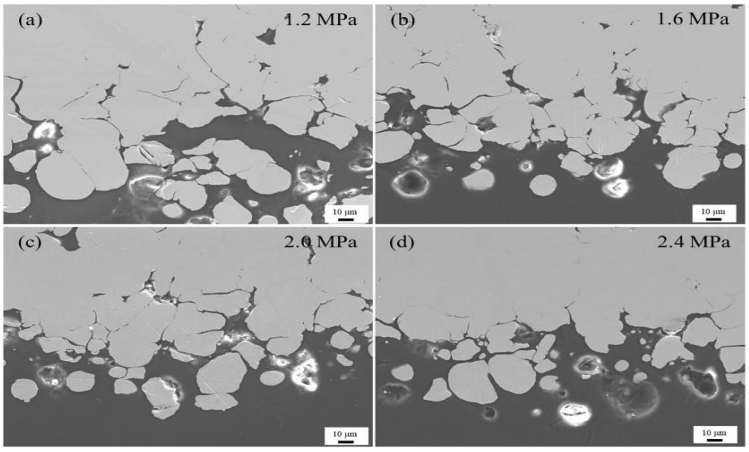

Fig. 18. Magnified view of the bond interface between the coating and the PEEK substrate at different propellant gas pressures: a) 1.2 MPa; b) 1.6 MPa; c) 2.0 MPa; d) 2.4 MPa [86].

Rija Nirina Raoelison, [87] investigated the strength of a copper/PEEK interface produced by a high-pressure cold spray and analyzed the effect of material dissymmetry by comparing this hybrid case with a copper/copper combination.
With the processing conditions specified in (Tables 2, 3), the deposition of copper powders on the PEEK substrate gives a DE of 79%. Copper-on-copper deposition is a common case in the literature that provides a sufficient characterization of the coating layer formation. It is known that the metal pair association generates a first layer through a metallurgical bond due to adiabatic shear when the powders collide on the substrate at a high strain impact rate. The plastic deformation during the collision thus causes bonding of the powders that reach the critical velocity, while the other powders bounce off the substrate due to insufficient impact velocity. This behavior explains the difference in DE value between the Cu/Cu and Cu/PEEK cases. The DE is slightly lower for the Cu/Cu case because of the rebound phenomenon. The PEEK substrate, which is softer than copper, has the ability to reduce the rebound phenomenon by absorbing the deformation during the collision, so that the powders penetrate the substrate instead of rebounding. The penetrated zone characterizes an intermediate layer of solder over a distance of up to 100µm at the Cu/PEEK interface (Fig. 19a). This layer produces adhesion of the copper layer by mechanical anchoring. Copper powders penetrating into the PEEK material are clearly observed, (Fig. 19b). The copper powders are weakly deformed and agglomerated with no apparent cohesion between them. Some powders are almost spheroidal, and others are only weakly flattened due to the deformation of the PEEK substrate, while in the case of the copper substrate, the flattening of all copper powders is significant. Instead of an anchored intermediate zone, as observed at the Cu/PEEK interface, the Cu/Cu interface consists of an abrupt transition, as the powders have not indented the copper substrate, but are significantly flattened (Fig. 20a). The detachment of the Cu layer from the Cu substrate also reveals this deformation (Fig. 20b).

Table 2. High pressure cold spray deposition conditions, [87]

Gas	P_{gas}, [bar]	T_{gas}, [°C]	SoD, [mm]	V_{nozzle}, [mm/s]	$Increment_{nozzle}$, [mm]
Air	30	400	135	100	3

Table 3. Details of the granulometry of the powdered raw material, [87]

Powder	Size range, [µm]	d10, [µm]	d50, [µm]	d90, [µm]
Cu	10-63	17.60	27.92	43.54

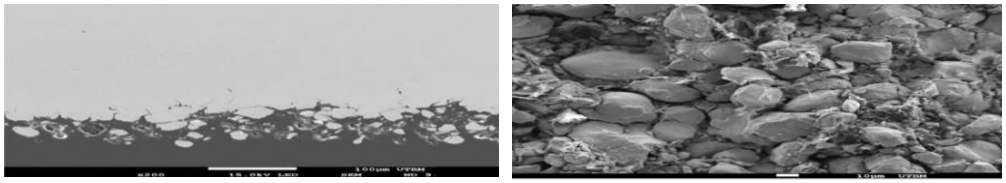

a) b)

Fig. 19. The characteristics of the intermediate penetrated zone at the Cu/PEEK interface: a) penetration of copper powders over an area of about 100 µm thickness; b) weakly deformed zone due to PEEK deformation [87].

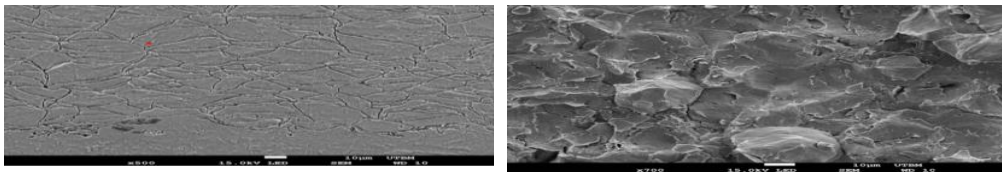

a) b)

Fig. 20. Deformation of copper powders: a) accentuated on the copper substrate; b) significant flattening evidenced by the detachment of the copper layer from the copper substrate [87].

2.2.7. Comparison between cold spraying on CFRP and Cu panel substrates

Figure 21 compares the DE of the Cu powder on the two different substrates; the gas temperature was set at the Inovati system's maximum, 482 °C, and the gas pressure was varied from 0.41 MPa to 0.46 MPa. In the case of electrodeposited CFRP, deposition occurred at pressures below 0.48 MPa, where the DE is about five times higher than that of the Cu panel for all sputtering conditions. The maximum DE of Cu powder on electroplated CFRP was 10%, which was obtained at a pressure of 0.46 MPa. A very slight increase (from 1.35% to 1.9%) in the deposition efficiency was observed for Cu panels with increasing gas pressure from 0.41 MPa to 0.46 MPa.

Cold spray deposition has been limited to pressures below 0.41 MPa. The reason could be that the particles do not exceed the critical velocity for deposition, as the critical velocity of copper particles is relatively high and has been reported to be on the order of 500 m/s [88].

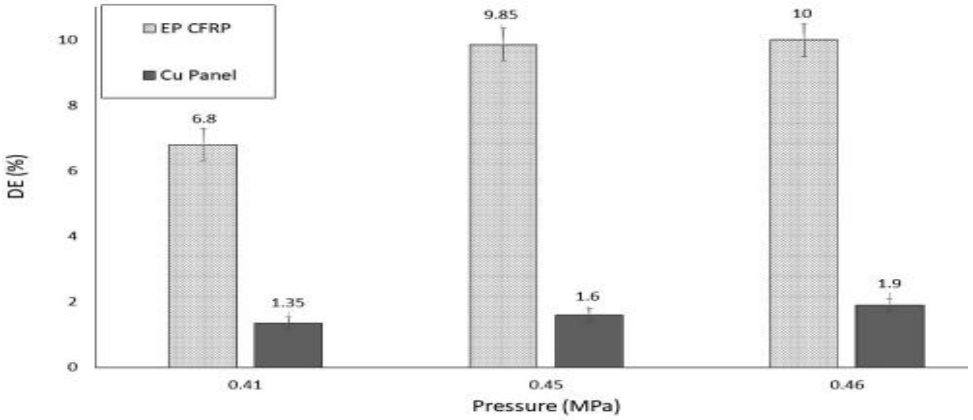

Fig. 21. Comparison of the Cu deposition efficiency at different pressures (0.41; 0.45; 0.46 MPa) for two different substrates (Cu electroplated CFRP and Cu sandblasted Cu panel) [88].

Similarly, Fukumoto et al [89] cold-sprayed copper on a stainless steel substrate for a gas pressure range from 1 MPa to 3 MPa at a gas temperature of 673 K. They confirmed that the coating deposition efficiency at a pressure of 1 MPa was very low (close to zero). It increased to about 40% at a pressure of 3 MPa, due to the improved mechanical interlock between the particles and the substrate. In this study, the notable variation in DE for the two substrates is investigated by analyzing the surface hardness and topology.

Hardness effect

The microhardness of raw material powder, Cu-electroplated CFRP, Cu panels and cold-sprayed Cu coatings are shown in Fig. 22. In previous studies [90, 91] it has been shown that the deposition behavior depends on the relative deformability of the particle with respect to the substrate. In a system in which the particles are more deformable than the substrate (i.e. soft particles/hard substrate), a higher degree of deformation takes place in the particle, leading to flattening of the particle. In the case of CFRP with galvanized Cu/Cu particles, it is possible that plastic deformation of both materials occurs during impact due to the similarity of hardness values (Fig. 22). However, in the case of impact of the Cu particle on a harder substrate (e.g. copper panel), the impact particles may undergo a higher degree of deformation relative to the substrate and a flattened particle may be formed on a slightly deformed substrate. Consequently, the presence of a softer copper interlayer, compared to the Cu panel, facilitated particle penetration and impact, allowing a better mechanical bonding between the particle and the substrate. It can also be observed in Fig. 22 that the microhardness of the cold-sprayed Cu layers increased from 100 HV to 118 HV with increasing gas pressure from 0.41 MPa to 0.46 MPa.

The deposited Cu particles underwent more plastic deformation by increasing gas pressure (higher particle velocity); therefore, a higher microhardness of the cold-sprayed Cu layer was obtained due to the increase in the hardening effect. No

cracking signs were observed around the indentation in the images of the indentations in Fig. 23.

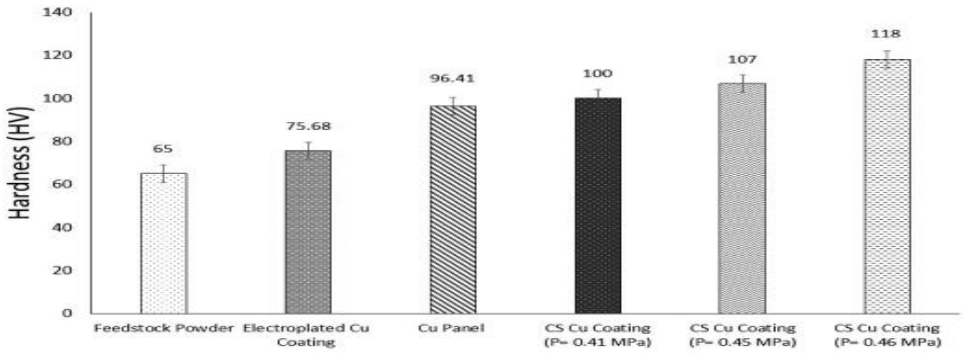

Fig. 22. Comparison of the microhardness of raw material powder, galvanized Cu layer, Cu panel and cold-sprayed Cu layers at different pressures (0.41; 0.45; 0.46 MPa) [90, 91].

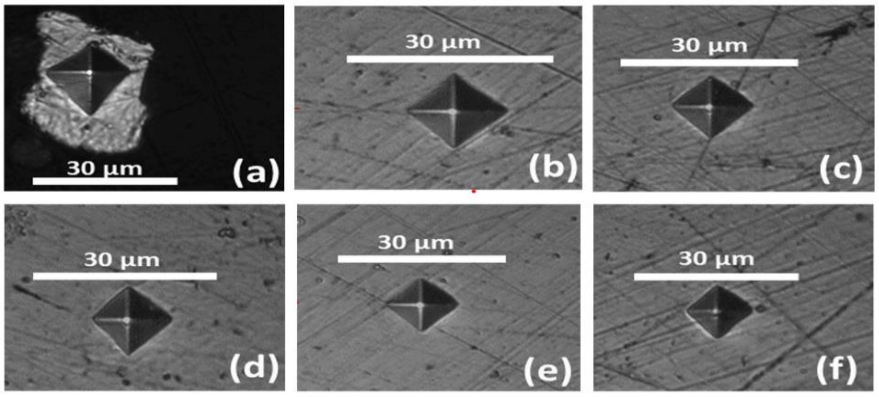

Fig. 23. Indentation micrographs of the deformed areas: a) of Cu powder; b) of galvanized Cu coating; c) of Cu panel; d) of cold-sprayed Cu coatings at different pressures 0.41 MPa, e) 0.45 MPa; f) 0.46 MPa under a load of 10 gf for a penetration time of 15 s [90, 91].

2.2.8. Mechanical properties of coated polymers

Aleksandra Małachowska et al [92], studied the metallization of polymers using low-pressure cold spray and determined the adhesion of the deposited layers.

The adhesion strength of the copper coatings was (3.6 ± 0.2) MPa. The first breaks occurred partially in the interlayer and partially in the coatings (Fig. 24). The authors of [93] reported that the bond strength of dendritic copper sprayed by low-pressure cold spray (pressure of 0.6 MPa and temperature of 540 °C) was ~7.5 MPa. This increased significantly to ~17.5 MPa with the addition of 50% Al_2O_3.

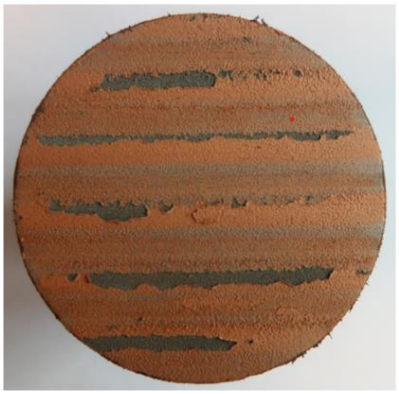

Fig. 24. Fracture after bond strength test [92].

The mechanism of adhesion and coating strength are usually attributed to two main mechanisms: the formation of shear instabilities at the particle/substrate and particle/particle interface, caused by extensive plastic deformation during impact [94, 95] and mechanical locking [96]. However, in the case of polymer/metal bonding, only the latter may occur due to the different nature of the coating material and the substrate material. Furthermore, "the interlocking may not be as strong as that observed on the metal substrate due to the soft nature of the polymer" [97]. Sn was found to have a more beneficial influence on bond strength. Ganesan et al. [98, 97], attributed this to the low mechanical properties of the tin particles, which were able to undergo deformation rather than surface damage. This initial intermediate layer then allowed bonding or interleaving for subsequent layers with higher mechanical properties, e.g. copper. In the case of spherical copper particles, the shear strength of the copper layer was (1.93 ± 0.7) MPa compared to (5.4 ± 0.9) MPa for the tin interlayer [97]. The adhesion strength obtained lies in the middle between these two values. The deposited copper coatings achieved a microhardness of $125HV_{0.1}$ ± 12 on PA6. This value is much lower than that given by Sudharshan - 300 or even $450HV_{0.1}$ for copper coatings on aluminum [99], but similar to the values given by [93, 97]. However, due to the different loads used for the measurements, the values cannot be directly compared. The low copper microhardness values could be attributed to a low degree of deformation of the base material. In addition, the lower microhardness of the coating material after heat treatment results in lower coating microhardness values.

2.3. Thermal spraying

S. Nigam et al [100] have studied copper thermal arc sputtering coating. Thus, Figure 25(a) shows the optical micrograph for cross-sectional view of the coated ABS parts showing three distinct layers. Figure 25(b) shows cross-sectional SEM images of the sputtered ABS part from 170mm, in which the coating layer thickness of about (175 ± 5) µm. This also includes the EDS analysis, [101].

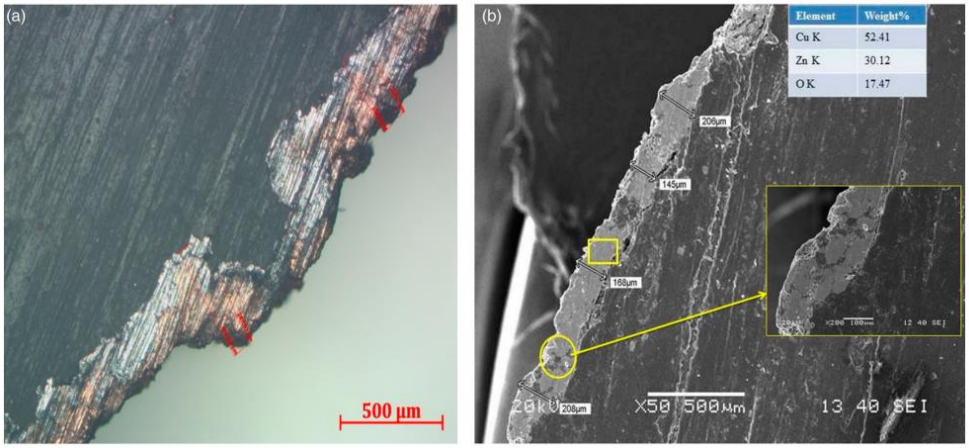

Fig. 25. SEM images of copper thermal spray coating: a) Optical micrograph showing three distinct layers of ABS, Zn and Cu; b) SEM images showing cross-sectional view of Cu-coated ABS, together with EDS analysis [101].

According to Figure 26, the reincorporation of circular rebound particles are those that affect the surface roughness the most, [102].

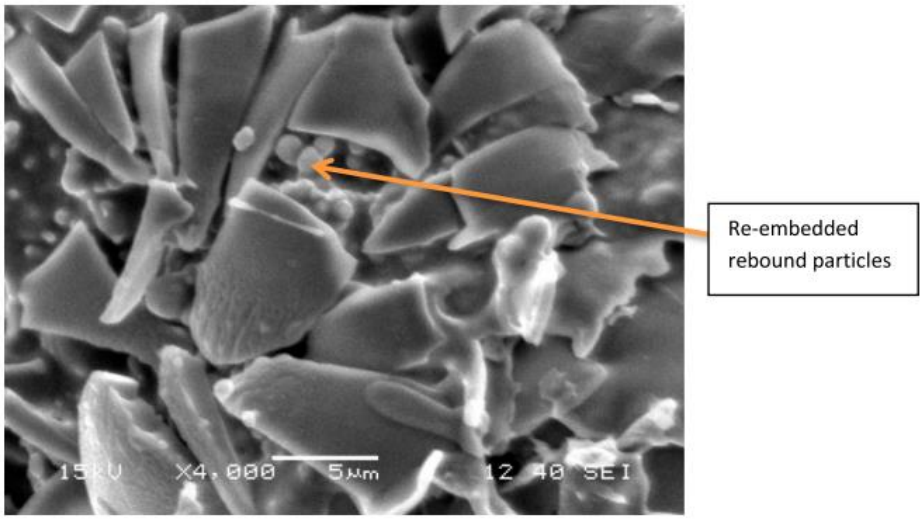

Fig. 26. SEM micrograph showing reincorporated ricochet particles [102].

Figure 27 shows a microstructure (SEM) of the sputtered 130mm sample, accompanied by EDS spectra. According to the EDS spectra, the coating consists of 2.4% oxygen and 97.6% copper. The EDS results are presented in Table 4 according to which the weight percent of oxygen varies between 1.6 and 14.7, showing an increasing trend as the SOD increases from 110 to 230 mm. With the

increase in SOD, a prolonged duration of interaction between the molten copper droplets and the surrounding environment results, [103].

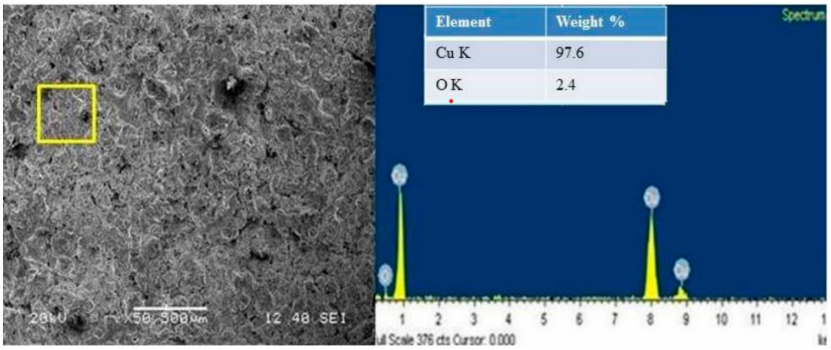

Fig. 27. EDS spectra of the top surface of the sprayed coating at a distance of 130mm [103].

Table 4. Composition of coated ABS parts, [103]

	Weight % of each element	
Stand-off distance, [mm]	Cu K	O K
110	98.3	1.6
130	97.6	2.4
150	97.4	3.6
170	95.6	4.4
190	90.2	9.8
210	89.8	10.2
230	85.600	14.40

Figure 28 shows the coating layer thickness and porosity content for each coated ABS part relative to SOD. At a spray distance greater than 150mm, oxidation occurs and the particles tend to solidify en route before reaching the substrate, due to the increase in porosity with increasing coating distance. However, at small coating distances (110-150)mm, particles reach the substrate at excessively high temperatures and/or velocities and, as a result, scatter and break upon impact, causing higher porosity. For a 150mm SOD, a stable equilibrium is observed. In this case, the maximum coating thickness influences the maximum porosity. For this reason, the coating layer sputtered from a distance of 230mm has a thickness of 269µm, which is the largest of all. Similarly, with SOD of (150-170)mm resulted a deposition of the coating layer with minimum thickness, [104].

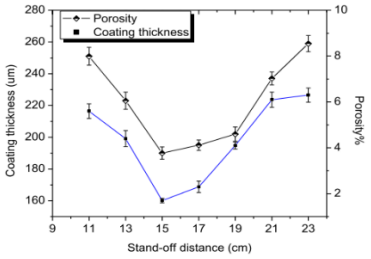

Fig. 28. Variation of coating thickness (µm) and porosity (%) as a function of spray distance [104].

Surface roughness

The surface roughness parameter (Ra) varies in the range (9-22) µm The value of Ra is lowest at 150mm SOD as shown in Figure 29. The surface roughness value decreases as the spray distance increases from 110mm to 150mm. However, with increasing SOD, there is an increase in surface roughness It has been reported that at longer spray distance the isotherms start to decompose faster, leading to partial melting of the particles, which means higher surface roughness, [105].

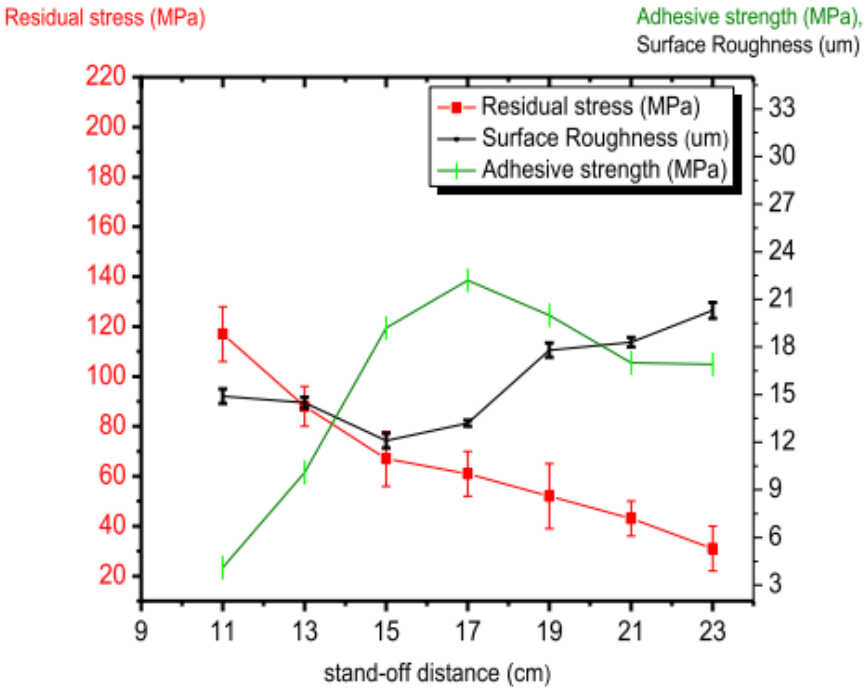

Fig. 29. Variation of adhesion strength, surface roughness and residual stress as a function of spray distance [105].

2.4. Formation of Cu crystals on the ABS surface

In their study Sushanta Kumar Sahoo et al., [106] observed copper crystals on the flat ABS surfaces for different acid baths at room temperature as shown in Figures

30, 31 and 32 (SEM images). Only in HF bath Cu crystals are formed on the ABS surface after 2 h of deposition as shown in Fig.30. After 24 h of deposition time, uniform Cu deposition was observed in the HF, H_2SO_4 and H_3PO_4 baths, as shown in Fig. 31, with a regular diamond pyramidal structure. As the deposition time gradually increases, the size of Cu crystals continues to increase, as shown in Fig. 32.

After a long deposition time, a metallic luster was observed due to the formation of large and uniform Cu crystals on the ABS surface.

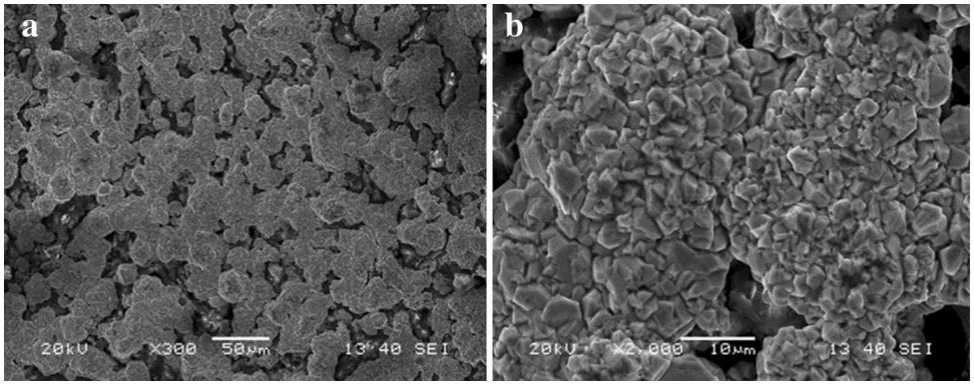

Fig. 30. SEM image of Cu crystals electrolytically deposited on ABS surfaces after 2 h for HF bath at room temperature: a) magnification 300, b) magnification 2000 [106].

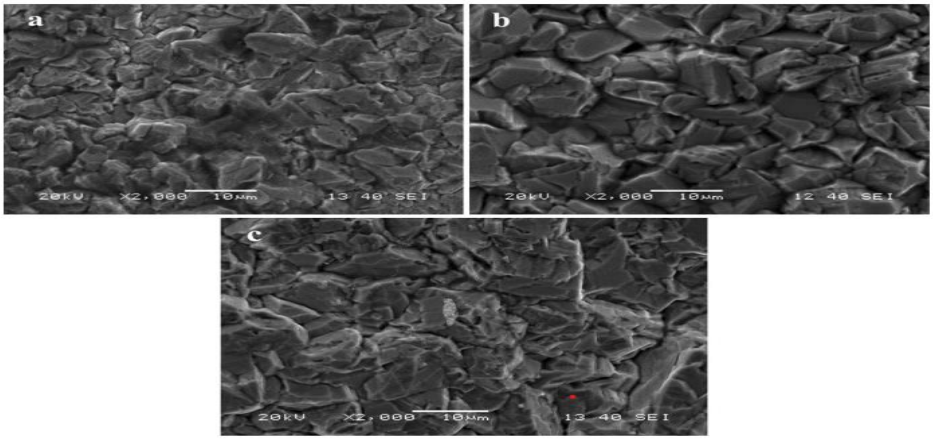

Fig. 31. SEM image of Cu crystals electrolytically deposited on ABS surfaces after 24 h at room temperature: a) HF bath; b) H_2SO_4 bath; c) H_3PO_4 bath [106].

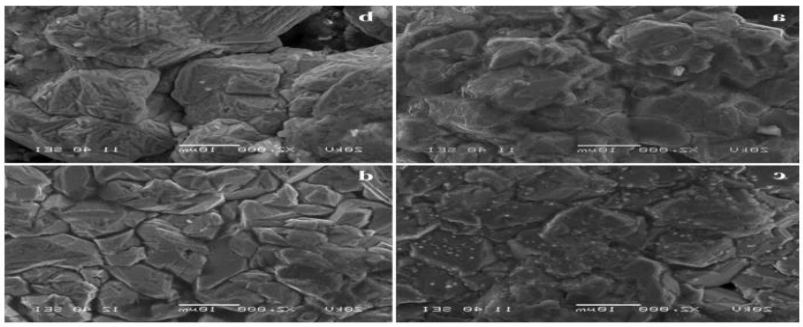

Fig. 32. SEM image of Cu crystals electrolytically deposited on ABS surfaces after 48 h at room temperature: a) H_2SO_4 bath; b) H_3PO_4 bath; c) HNO_3 bath; d) CH_3COOH bath after 72 h [106].

2.4.1. Characterizing EDS

The EDS spectra of ABS samples electrodeposited with Cu in different baths at room temperature are examined as shown in Figures 33, 34, 35, 36 and 37. For HF, H_2SO_4, H_3PO_4 and HNO_3 baths, EDS is performed after 48 h of deposition, but for $CH3COOH$after 72 h. All surface elements are analyzed by EDS mapping by peak searching. The results indicate that Cu is dominant at the surface in all electrolyte baths, but considerable deposition is corresponding for HF, H_2SO_4, H_3PO_4 and HNO_3 baths. Elemental analysis of Cu-deposited ABS surfaces was also performed and the elemental compositions are presented. For the HF and H_2SO_4 baths, the Cu content appears at a level of 81.11% and 83.58 wt%, respectively, while the copper content appears at a wt% of 76.24% and 70.69% for the H_3PO_4 and HNO_3 baths, respectively. Even after 72 hours of deposition, the weight percent of copper deposition for CH_3COOHbath is only 57%. With the exception of the CH3COOHbath, the others produced more than 70 wt% copper on the ABS surface.

A Carl Zeiss Carl Zeiss microscope was used to measure the thickness of the Cu coated ABS parts. The thickness varied from place to place on the surface. Figure 38 shows the copper thickness measured for the $H2SO4$ bath after 48 h of deposition. The Al and copper layers are clearly visible in the figure with a copper thickness of 64.04 µm. The Cu thickness is further increased by electroplating, [108].

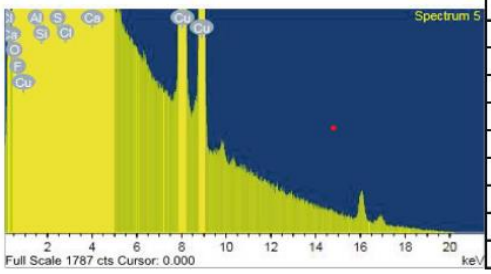

HF		
Element	Weight%	Atomic%
O K	11.55	31.36
F K	3.25	7.44
Al K	1.44	2.32
Si K	0.33	0.51
S K	0.92	1.25
Cl K	1.02	1.25
Ca K	0.38	0.41
Cu K	81.11	55.47
Total	100	

Fig. 33. EDX for different copper coatings in HF bath: a) EDX spectra; b) elemental analysis of ABS sample [106].

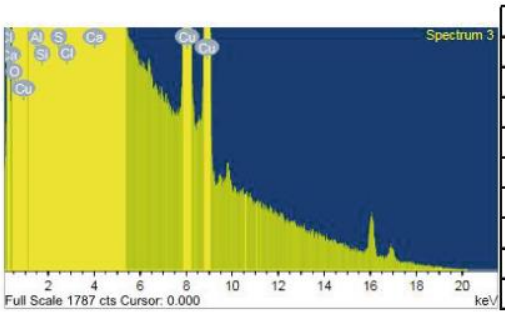

H2SO4		
Element	Weight%	Atomic%
O K	12.27	34.54
Al K	1.67	2.79
Si K	0.72	1.15
S K	0.62	0.87
Cl K	0.77	0.98
Ca K	0.37	0.42
Cu K	83.58	59.25
Total	100	

Fig. 34. EDX for different copper coatings in H_2SO_4 bath: a) EDS spectra; b) Elemental analysis of ABS sample [107].

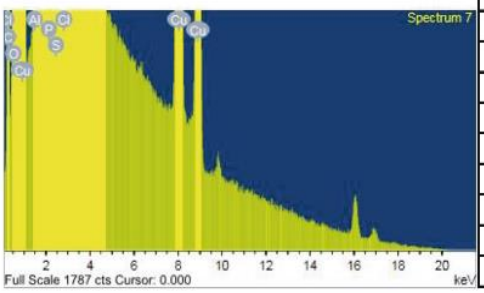

H3PO4		
Element	Weight%	Atomic%
C K	15.09	42.66
O K	6.75	14.32
Al K	1.33	1.68
P K	0.19	0.21
S K	0.23	0.24
Cl K	0.17	0.17
Cu K	76.24	40.73
Total	100	

Fig. 35. EDX for different copper coatings in H_3PO_4 bath: a) EDS spectra; b) elemental analysis of ABS sample [107].

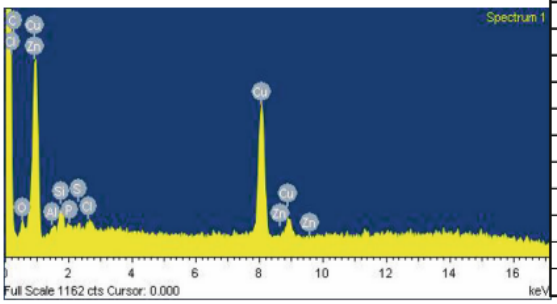

HNO3		
Element	Weight%	Atomic%
C K	14.98	42.19
O K	4.9	10.36
Al K	1.49	1.87
Si K	3.49	4.21
P K	0.94	1.03
S K	0.67	0.71
Cl K	1.22	1.17
Cu K	70.69	37.64
Zn K	1.61	0.83
Total	100	

Fig. 36. EDX for different copper coatings in HNO_3 bath: a) EDS spectra; b) elemental analysis of ABS sample [107].

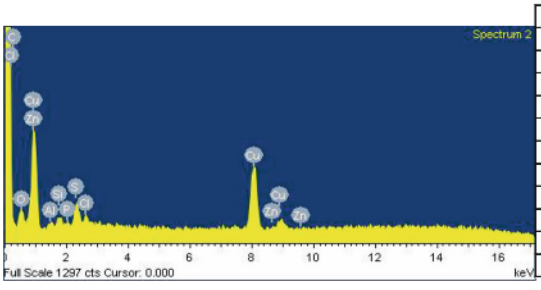

CH3COOH		
Element	Weight%	Atomic%
C K	17.49	41.28
O K	12.63	22.38
Al K	1.44	1.51
Si K	2.25	2.27
P K	0.75	0.69
S K	4.76	4.21
Cl K	1.72	1.38
Cu K	57	25.43
Zn K	1.94	0.83
Total	100	

Fig. 37. EDX for different copper coatings in CH_3COOHbath: a) EDS spectra; b) elemental analysis of ABS sample [107].

Fig. 38. Cu layer thickness on ABS surface [108].

2.4.2. Characterization of composites

Piotr Rytlewski et al, [109], evaluated the possible application of microscopic copper particles as a metallization precursor for ABS by LDS technique.

High impact strength and modulus of elasticity, ease of processing and common applications in electroless metallization and 3D additive manufacturing motivated the use of ABS as a matrix for composites intended for selective laser-assisted metallization and 3D printing applications. On the other hand, the high sensitivity to thermal, oxidative and/or UV-induced degradation can be identified as disadvantageous.

The applied copper was presented as a powder with irregular spherical shaped particles with diameters ranging from about 3 μm to 20 μm. Initially, DSC tests were performed to determine the possible effect of copper on the ABS structure. Due to the styrene (S), acrylonitrile (AN) and B blocks, three characteristic phase transitions can be expected. The glass transition of the B phase (at about -53 ◦C [110] or even at about -80 ◦C [111]) is difficult to detect by DSC, even using high heating/cooling rates.

The results of the TG analysis revealed that, for all samples examined, the values of the degradation onset temperature () and the temperature (TMax) at the maximum rate of mass loss were similar. However, as the concentration of copper increased, the process came to an end at significantly lower temperatures (TEnd), suggesting that copper can accelerate the ABS degradation process even in the absence of oxygen. Table 5 contains the values of these temperatures for every sample that was tested, and Figure 39 displays the chosen TG/DTG curves.

Table 5. Temperatures at the beginning (T_{On}), end (T_{End}) and maximum speed (T_{Max}) mass loss determined from DTG curves for the samples studied, [109]

Samples	T_{On}, [°C]	T_{Max}, [°C]	T_{End}, [°C]
A	389	428	475
B	382	428	466
C	385	429	467
D	386	429	466
E	383	424	465

Additionally, it was noted that the DTG for pure ABS was obviously asymmetric (having two local maxima), whereas in the samples containing copper, there was only one discernible maximum (at about 424 ◦C). The overlap between SAN fractions and PB degradation explains this asymmetry. The TG curve has considerable asymmetry due to the well-known fact that the PB phase begins to deteriorate before the SAN phase, even though both degradation processes typically overlap [112]. This imbalance for the TG curves should be lessened since copper-filled samples, which transport heat more effectively, should experience more dynamic deterioration processes for both the PB and SAN phases. It is well known that ABS can lose its impact strength when exposed to heat [113]. However, a Charpy impact test does not generally produce significant differences in impact values [114].

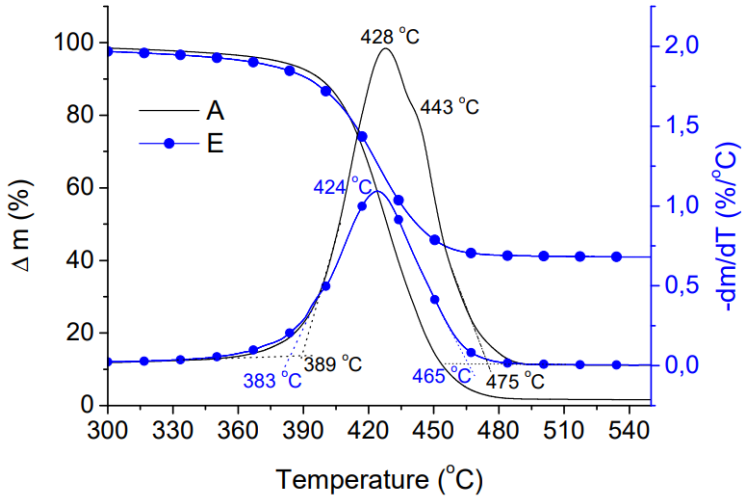

Fig. 39. TG/DTG analysis for samples A and E, [109]

As shown in Table 16, theEB values increased from about 16 to about 33 kJ/m^2 after the addition of 0.6 vol% Cu, while with further increase of Cu (4.8 vol%) they were reduced to about 15 kJ/m$^{2.}$ The presence of copper was found to be insignificantly detrimental to the ABS fracture toughness. The clean ABS had anEB of approximately 16 kJ/m^2. On addition of a small amount of Cu theEB value increased to about 33 kJ/m^2; with further increase in Cu content theEB was observed to decrease to about 15 kJ/m^2, (Table 6).

Higher Cu content made ABS stiffer, and Young's modulus values were inversely correlated withEB. The melt flow velocity of the samples decreased from about 27 to about 10 with increasing copper content. This significant reduction in MFR may require higher processing temperatures in certain manufacturing techniques (especially for thin-walled injection molded or 3D printed products). On the other hand, a higher processing temperature may lead to more intense degradation of these composites, as demonstrated in this work.

Table 6. Young's modulus (E), tensile strength (σM), strain at σM, (εM), tensile strain at break (σB), strain at σB (εB), breaking energy (EB), melt flow rate (MFR) of the studied samples [114].

Sample	E(MPa)	σ_M (MPa)	ε_M(%)	σ_B (MPa)	ε_B(%)	E_B(kJ/m^2)	MFR^{o}C;5kg
A	1143±20	33.2±1.9	4.93±0.38	23.7±5.0	7.0±1.1	16.3±1.6	26.5±0.9
B	1082±38	39.3±1.7	6.80±0.21	38.8±1.6	7.0±1.3	33.0±2.5	21.9±0.6
C	1103±22	36.9±1.7	5.42±0.32	36.9±1.8	5.4±0.4	24.6±2.4	16.5±0.5
D	1276±17	36.3±1.6	4.80±0.31	33.8±3.9	5.2±0.3	21.7±1.5	12.0±0.8
E	1398±24	32.5±1.6	3.92±0.25	30.2±3.6	4.2±0.3	14.9±1.2	10.0±0.5

3. Conclusions

Because plastics have properties such as light weight, corrosion resistance, high strength-to-weight ratio, good durability, low cost and ease of manufacture, they have wide application in industry and the household sector.

In particular, the automotive, electronics and aerospace industries make extensive use of plastic parts. But plastic cannot be used directly when metal-like properties such as electrical conductivity, surface hardness and thermal conductivity are required for products. These requirements can be achieved by realizing metallic coatings on plastic surfaces to replace metals in different industries.

The development of conductive coating on a non-conductive material is known as metallization which combines the properties of both plastic and metal.

Metallization is used to make decorative products, circuit boards and components used in the automotive, aviation and shipbuilding industries.

The metallization of polymers can be divided into three categories based on the fission principle used, as follows: atomic deposition of metals in a plasma or electrolyte; sputtering of metal powder; and direct thermal fusion.

These different categories can be complemented in a single set of tools for any polymer metallization application to enable the realization of metal layers with thicknesses ranging from nanometers to millimeters.

By understanding the advantages and disadvantages of the listed methods, several hybrid methods can be developed. In all of these techniques, a common critical issue is encountered: how to ensure the required level of adhesion at the polymer-metal interface so that the integrity of the application is not compromised in the long term. It has been found that chemical bonding can maintain a metal film at the nanoscale, but is considered insufficient for use in thick metal layers at the micro and macro scale.

Polymers can be coated using several thermal spraying methods: flame spraying, arc spraying, plasma spraying and cold spraying.

CS (cold spray) deposition of metallic coatings on polymers and composites is an innovative process. Since its inception a decade ago, it has gained momentum due to the global spread of polymer parts in various industries. This technique can metallize any polymer (thermoset, thermoplastic and composite, including fibre-reinforced composites). Direct polymer-metal bonding achieves PM layers with millimetre-scale thicknesses and can enable the realization of macroscopic-scale hybrids.

In order to assess the state of the art in the field of polymer metallization by CS, more than 50 articles on CS deposition of metals on polymers were reviewed and the conclusions are presented below:
- CS enables the rapid deposition of conductive and adherent metal coatings on various thermoplastic materials and attachment thermopolymers respectively fiber-reinforced composites. Both low-pressure and high-pressure CS systems have been successfully used.
- CS on polymers has a very limited range of process parameters. The effects of most of the process parameters on the physical process factors are known qualitatively. As a next step, fundamental models should be developed to quantify the physical factors required to form the coating layer. Once the values of these physical factors are known, the powder and spray parameters can be easily adjusted and optimized.
Most research in the field of CS has focused on the adhesion strength and CE of the coating. The bond strength of most polymers and powdered metals used in CS ranges from 2 to 10 MPa, which is considerably higher than other polymer surface coating approaches.
Plasma-based copper coating technology is an efficient, flexible and repeatable technology to create a direct copper coating. The process is suitable for both prototyping and industrial scale production.
Thermal spray methods are predominantly used for thick film deposition of soft metals.
Compared to other coating technologies, thermal spray methods offer certain advantages as well as unique coating characteristics and process capabilities, as follows:
-High coating deposition rate (up to 100 μm/s);
-Cost efficiency: cheap consumables, simple maintenance and easy personal training;
-Variable coating thickness (micro to millimeter scale);
-Superior coating adhesion strength (up to 20 MPa);
-Customizedcoating qualities: porosity, hardness, conductivity and bioactivity;
-High process stability: lineardeposition rate, vibration and wear free;
-One-step process: eliminates the need for cleaning, grease removal, surface roughening, thermal pretreatment, masking and other pretreatments;
-Ecology: requires no rare materials, produces no hazardous waste;
-Hybridization: thermal spraying is easily combined with other processing methods, e.g. cold spraying with selective laser melting or abrasive jet for additive manufacturing or material replacement respectively.
Thermal spray methods also have disadvantages that limit their use, as follows:
-Only soft metals are recommended for direct sprayed coatings. Hard metals should be sprayed on soft intercoats;
-Structural, mechanical and electrical properties of the coating are inferior to those of the base material and the coatings are rough and porous;
-Thermal spray metal coatings are still under-researched;

-Lack of fundamental understanding of the process-material-property relationship requires pilot experiments and optimization of the polymer spray process in each case.

References

[1] Polymers Market - Forecast (2020 - 2025), Res. Mark, 2020. https://www.researc handmarkets.com/reports/5021563/.
[2] Hsissou R., Seghiri R., Benzekri Z., Hilali M., Rafik M., Elharfi A., *Polymer composite materials: a comprehensive review*, Compos. Struct., **262**, 2021, 113640.
[3] Prucz J., Shoukry S., William G., Shoukry M., *Lightweight Composite Materials for Heavy Duty Vehicles*, West Virginia University, 2013.
[4] Brinson H.F., Brinson L.C., *Polymerization and classification, in: Polymer Engineering Science and Viscoelasticity*, Springer, Boston, MA, 2008, p. 99–157.
[5] Mavukkandy M.O., McBride S.A., Warsinger D.M., Dizge N., Hasan S.W., Arafat H. A., *Thin film deposition techniques for polymeric membranes – a review*, J. Memb. Sci., **610**. 2020, 118258.
[6] Ferreira A.A., Silva F.J.G., Pinto A.G., Sousa V.F.C., *Characterization of thin chromium coatings produced by PVD sputtering for optical applications*, Coatings, 11, 2021 p. 1–20.
[7] Shacham-Diamand Y., Osaka T., Okinaka Y., Sugiyama A., Dubin V., *30 Years of electroless plating for semiconductor and polymer micro-systems*, Microelectron. Eng., **132**, 2015, p. 35–45.
[8] Ghosh S., *Electroless copper deposition: a critical review*, Thin Solid Films, **669**, 2019, p. 641–658.
[9] Petrovicova E., Schadler L.S., *Thermal spraying of polymers*, Int. Mater. Rev., **47**, 2002, p. 169–190.
[10] Gonzalez R., Ashrafizadeh H., Lopera A., Mertiny P., McDonald A., *A review of thermal spray metallization of polymer-based structures*, J. Therm. Spray. Technol., **25**, 2016, p. 897–919.
[11] Fotovvati B., Namdari N., Dehghanghadikolaei A., *On coating techniques for surface protection: a review*, J. Manuf. Mater. Process, **3**, 22, 2019, https://doi. org/10.3390/jmmp3010028.
[12] Sturgeon A., Dunn B., Celotto S., O'Neill B., *Cold sprayed coatings for polymer composite substrates*, Eur. Sp. Agency, Special Publ. ESA SP., 2006, p. 19–23.
[13] Irissou E., Legoux J.G., Ryabinin A.N., Jodoin B., Moreau C., *Review on cold spray process and technology: part I - intellectual property*, J. Therm. Spray. Technol., **17**, 2008, p. 495–516.
[14] Singh H., Sidhu T.S., Kalsi S.B.S., *Cold spray technology: future of coating deposition processes*, Frat. Ed. Integrita Strutt., **22**, 2012, p. 69–84.
[15] Luo X.T., Li C.X., Shang F.L., Yang G.J., Wang Y.Y., Li C.J., *High velocity impact induced microstructure evolution during deposition of cold spray coatings: A review*, Surf. Coat. Technol., **254**, 2014, p. 11–20.
[16] Moridi A., Hassani-Gangaraj S.M., Guagliano M., Dao M., *Cold spray coating: review of material systems and future perspectives*, Surf. Eng., **30**, 2014, p. 369–395.
[17] Fardan A., Berndt C.C., Ahmed R., *Numerical modelling of particle impact and residual stresses in cold sprayed coatings: a review*, Surf. Coat. Technol., **409**, 202, 126835.
[18] Sample C.M., Champagne V.K., Nardi A.T., Lados D.A., *Factors governing static properties and fatigue, fatigue crack growth, and fracture mechanisms in cold spray alloys and coatings/repairs: a review*, Addit. Manuf., **36**, 2020, 101371.
[19] Li W., Cao C., Yin S., *Solid-state cold spraying of Ti and its alloys: a literature review*, Prog. Mater. Sci., **110**, 2020, 100633.
[20] Huang B., Zhang C., Zhang G., Liao H., *Wear and corrosion resistant performance of thermal-sprayed Fe-based amorphous coatings: a review*, Surf. Coat. Technol., **377**, 2019, 124896.
[21] Yin S., Cavaliere P., Aldwell B., Jenkins R., Liao H., Li W., Lupoi R., *Cold spray additive manufacturing and repair: fundamentals and applications*, Addit. Manuf., **21**, 2018, p. 628–650.
[22] Raoelison R.N., Xie Y., Sapanathan T., Planche M.P., Kromer R., Costil S., Langlade C., *Cold gas dynamic spray technology: a comprehensive review of processing conditions for various technological developments till to date*, Addit. Manuf., **19**, 2018, p. 134–159.

[23] Parmar H., Tucci F., Carlone P., Sudarshan T.S., *Metallisation of polymers and polymer matrix composites by cold spray: state of the art and research perspectives*, Int. Mater. Rev., 0, 2021, p. 1–25.
[24] Yu N., Jourdain R., Castelli M., Bennett A., Guo J., Ma C., Fang F., *Investigation of a plasma delivery system for optical figuring process*, Chin. J. Aeronaut., **34**, 2021, p. 518–525.
[25] Zhou H., Bennett A., Castelli M., Jourdain R., Guo J., Yu N., *Design of a motorised plasma delivery system for ultra-precision large optical fabrication*, Int. J. Extrem. Manuf., **2**, 2020, 045301.
[26] Devaraj S., Anand B., Gibbons M., McDonald A., Chandra S., *Thermal spray deposition of aluminum and zinc coatings on thermoplastics*, Surf. Coat. Technol., **399**, 2020, 126114.
[27] Rezzoug A., Abdi S., Kaci A., Yandouzi M., *Thermal spray metallisation of carbon fibre reinforced polymer composites: effect of top surface modification on coating adhesion and mechanical properties*, Surf. Coat. Technol., **333**, 2018, p. 13–23.
[28] Kuroda S., Kawakita J., Watanabe M., Katanoda H., *Warm spraying - a novel coating process based on high-velocity impact of solid particles*, Sci. Technol. Adv. Mater., **9**, 2008, 033002.
[29] Zhang D., Shipway P.H., McCartney D.G., *Cold gas dynamic spraying of aluminum: the role of substrate characteristics in deposit formation*, J. Therm. Spray. Technol., **14**, 2005, p. 109–116.
[30] Affi J., Okazaki H., Yamada M., Fukumoto M., *Fabrication of aluminum coating onto CFRP substrate by cold spray*, Mater. Trans., **52**, 2011, p. 1759–1763.
[31] Agredo Diaz D.G., Valdez Navarro R.G., Ortiz Godoy N., Barba Pingarron A., ´ Gonzalez J. R.´ Parra, Olaya Florez J.J., Trujillo Barrag´ an M., Angarita Moncaleano I., Ortiz Otalora C.A., *Flame-sprayed Zn-Al coatings on ABS without chemical surface preparation*, Mater. Lett., **280**, 2020, p. 128574.
[32] Ashrafizadeh H., McDonald A., Mertiny P., *Deposition of electrically conductive coatings on castable polyurethane elastomers by the flame spraying process*, J. Therm. Spray. Technol., **25**, 2016, p. 419–430.
[33] Voyer J., Schulz P., Schreiber M., *Conducting flame-sprayed Al coatings on textile fabrics*, J. Therm. Spray. Technol., **17**, 2008, p. 583–588.
[34] Bin Lee H., Lin T.J., Lee C.Y., *Corrosion of high-velocity-oxygen-fuel (HVOF, sprayed non-crystalline alloy coating in marine environment*, Surf. Coat. Technol., **409**, 2021, 126896.
[35] Qiao L., Wu Y., Hong S., Cheng J., Wei Z., *Influence of the high-velocity oxygenfuel spray parameters on the porosity and corrosion resistance of iron-based amorphous coatings*, Surf. Coat. Technol., **366**, 2019, p. 296–302.
[36] Morgan R.H., Sutcliffe C.J., Pattison J., Murphy M., Gallagher C., Papworth A., Fox P., O'Neill W., *Cold gas dynamic manufacturing - a new approach to near-net shape metal component fabrication*, Mater. Res. Soc. Symp. Proc., **758**, 2003, p. 73–84.
[37] Yu N., Yang Y., Jourdain R., Gourma M., Bennett A., Fang F., *Design and optimization of plasma jet nozzles based on computational fluid dynamics*, Int. J. Adv. Manuf. Technol., **108**, 2020, p. 2559–2568.
[38] Yu N., Jourdain R., Gourma M., Shore P., *Analysis of De-Laval nozzle designs employed for plasma figuring of surfaces*, Int. J. Adv. Manuf. Technol., **87**, 2016, p. 735–745.
[39] Schmidt T., G¨ artner F., Assadi H., Kreye H., *Development of a generalized parameter window for cold spray deposition*, Acta Mater., **54**, 2006, p. 729–742.
[40] Ruslan Melentiev, Arief Yudhanto, Ran Tao, Todor Vuchkov, Gilles Lubineau, *Metallization of polymers and composites: State-of-the-art approaches*, https://doi.org/10.1016/j.matdes.2022.110958
[41] Sampath S., *Thermal spray applications in electronics and sensors: Past, present, and future*, J Therm Spray Technol., **19**, 2010, p. 921–949, ed WC – 12Co coatings. Mater Manuf Process., **29**, 2014, p. 1117–1125.
[42] Ashrafizadeh H., McDonald A., Mertiny P., *Deposition of Electrically Conductive Coatings on Castable Polyurethane Elastomers by the Flame Spraying Process*, J Therm Spray Technol., **25**, 2016, p. 419–430.
[43] Devaraj S., Anand B., Gibbons M., McDonald A., Chandra S., *Thermal spray deposition of aluminum and zinc coatings on thermoplastics*, Surf Coatings Technol, **399**, 2020.

[44] Rezzoug A., Abdi S., Kaci A., Yandouzi M., *Thermal spray metallisation of carbon fibre reinforced polymer composites: Effect of top surface modification on coating adhesion and mechanical properties*, Surf Coatings Technol, **333**, 2018, p. 13–23.
[45] Liu A., Guo M., Zhao M., Ma H., Hu S., *Arc sprayed erosion-resistant coating for carbon fiber reinforced polymer matrix composite substrates*, Surf Coatings Technol., **200**, 2006, p. 3073–3077.
[46] Ganesan A., Yamada M., Fukumoto M., *The effect of CFRP surface treatment on the splat morphology and coating adhesion strength*, J Therm Spray Technol., **23**, 2014, p. 236–244.
[47] Sun G., He X., Jiang J., Sun Y., Zhong Y., *A study on the deposition of Al_2O_3 coatings on polymer substrates by a plasma spray/micro-arc oxidation twostep method*, J Therm Spray Technol., **22**, 2013, p. 27–35.
[48] Sargin F., Erdogan G., Kanbur K., Turk A., *Investigation of in vitro behavior of plasma sprayed Ti, TiO_2 and HA coatings on PEEK*, Surf Coatings Technol., **411**, 2021.
[49] Ganesan A., Yamada M., Fukumoto M., *Cold spray coating deposition mechanism on the thermoplastic and thermosetting polymer substrates*, J Therm Spray Technol., **22**, 2013, p. 1275–1282.
[50] Koithara L.L., Raoelison R.N., Costil S., Xie X., *High deposition efficiency and delamination issues during high-pressure cold spraying metallization of PEEK using spherical copper powders*, Int J Adv Manuf Technol., **10**, 7, 2020, p. 4427–4436.
[51] Melentiev Ruslan, Yu Nan, Lubineau Gilles, *Polymer metallization via cold spray additive manufacturing: A review of process control, coating qualities, and prospective applications*.
[52] Che H., Vo P., Yue S., *Investigation of cold spray on polymers by single particle impact experiments*, J. Therm. Spray. Technol., **28**, 2018, p. 135–143.
[53] Ghelichi R., Guagliano M., *Coating by the Cold Spray Process: a state of the art*, Frat. Ed. Integrita ` Strutt., **8**, 2009, p. 30–44.
[54] Robitaille F., Yandouzi M., Hind S., Jodoin B., *Metallic coating of aerospace carbon/epoxy composites by the pulsed gas dynamic spraying process*, Surf. Coat. Technol., **203**, 2009, p. 2954–2960.
[55] Che H., Chu X., Vo P., Yue S., *Metallization of various polymers by cold spray*, J. Therm. Spray. Technol., **27**, 2018, p. 169–178.
[56] Ganesan A., Yamada M., Fukumoto M., *Cold spray coating deposition mechanism on the thermoplastic and thermosetting polymer substrates*, J. Therm. Spray. Technol., **22**, 2013, 1275–1282.
[57] Che H., Gagn´e H., Rajesh P.S.M., Klemberg-Sapieha J.E., Sirois F., Therriault D., Yue S., *Metallization of carbon fiber reinforced polymers for lightning strike protection*, J. Mater. Eng. Perform., **27**, 2018, p. 5205–5211.
[58] Gardon M., Latorre A., Torrell M., Dosta S., Ferndandez J., Guilemany J.M., *Cold gas spray titanium coatings onto a biocompatible polymer*, Mater. Lett., **106**, 2013, p. 97–99.
[59] Hanqing Che, Xin Chu, Phuong Vo, Stephen Yue, *Metallization of Various Polymers by Cold Spray*.
[60] Lupoi R., O'Neill W., *Deposition of metallic coatings on polymer surfaces using cold spra*y, Surf. Coat. Technol., **205**, 2010, p. 2167–2173.
[61] Villafuerte J., *Modern cold spray: materials, process, and applications*, *Mod. Cold Spray*. Mater. Process. Appl., 2015, p. 1–429.
[62] Raoelison R.N., Verdy C., Liao H., *Cold gas dynamic spray additive manufacturing today: deposit possibilities, technological solutions and viable applications*, Mater. Des., **133**, 2017, p. 266–287.
[63]. Perna A.S, Viscusi A., Astarita A., Boccarusso L., Carrino L., Durante M., Sansone R., *Manufacturing of a Metal Matrix Composite Coating on a Polymer Matrix Composite Through Cold Gas Dynamic Spray Technique*.
[64] Chu X., Che H., Yue S., *Understanding the cold spray deposition characteristics of mixed metal powders*, MRS Adv., **4**, 2019, p. 2989–2995.
[65] Che H., Chu X., Vo P., Yue S., *Cold spray of mixed metal powders on carbon fibre reinforced polymers*, Surf. Coat. Technol., **329**, 2017, p. 232–243.

[66] Bortolussi V., Borit F., Chesnaud A., Jeandin M., Faessel M., Figliuzzi B., Willot F., Roche K., G. Surdon, *Cold spray of metal-polymer composite coatings onto Carbon Fiber-Reinforced Polymer (CFRP*, Proc. Int. Therm. Spray Conf., **1**, 2016, p. 437–443.
[67] Stoltenhoff T., Kreye H., Richter H.J., *An analysis of the Cold Spray Process and its Coatings*, J. Therm. Spray Tech, 2002, **11**, 4, p. 542-550.
[68] Koivuluoto H., Vuoristo P., *Effect of powder type and composition on structure and mechanical properties of Cu+ Al_2O_3 coatings prepared by using low-pressure cold spray process*, J. Therm. Spray. Technol., **19**, 2010, p. 1081–1092.
[69] Rokni M.R., Feng P., Widener C.A., Nutt S.R., *Depositing al-based metallic coatings onto polymer substrates by cold spray*, J. Therm. Spray. Technol., **28**, 2019, p. 1699–1708.
[70] Irissou E., Legoux J.-G., Arsenault B., Moreau C., *Investigation of Al-Al2O3 Cold Spray Coating Formation and Properties*, J. Therm. Spray Tech., 2007, **16**, 5-6, p. 661-668.
[71]. Che H., Vo P. and Yue S., *Metallization of Carbon Fibre Reinforced Polymers by Cold Spray*, Surf. Coat. Technol., **313**, 2017, p. 236-247.
[72] Stoltenhoff T., Kreye H., Richter H.J., *An analysis of the Cold Spray Process and its Coatings*, J. Therm. Spray Tech., **11**, 4, 2002, p. 542-550.
[73] Dykhuizen R.C. and Smith M.F., *Gas Dynamic Principles of Cold Spray*, J. Therm. Spray Tech., **7**, 2, 1998, p. 205-212.
[74] Zhou X.L., Chen A.F., Liu J.C., Wu X.K. and Zhang J.S., *Preparation of Metallic Coatings on Polymer Matrix Composites by Cold Spray*, Surf. Coat. Technol., **206**, 1, 2011, p. 132-136.
[75] Garcia Alexandre, Berthelot Thomas, Viel Pascal, Mesnage Alice, Jegou Pascale, Nekelson Fabien, Roussel Sebastien, Palacin Serge, *ABS Polymer Electroless Plating through a One-Step Poly(acrylic acid, Covalent Grafting*.
[76] Ganesan A., Yamada M. and Fukumoto M., *Cold Spray Coating Deposition Mechanism on the Thermoplastic and Thermosetting Polymer Substrat*es, J. Therm. Spray Tech, **22**, 8, 2013 p. 1275-1282.
[77]. Gardon M., Latorre A., Torrell M., Dosta S., Fernandez J., Guilemany J.M., *Cold Gas Spray Titanium Coatings onto a Biocompatible Polymer*, Mater. Lett., **106**, 3, 2013, p. 97-99.
[78]. Zhou X.L., Chen A.F., Liu J.C., Wu X.K. and Zhang J.S., *Preparation of Metallic Coatings on Polymer Matrix Composites by Cold Spray*, Surf. Coat. Technol., **206**, 1, 2011, p. 132-136.
[79] Chaoyue Chena, Xinliang Xiea, Yingchun Xiea, Xincheng Yana, Chunjie Huanga, Sihao Denga, Zhongming Renc, Hanlin Liaoa, *Metallization of polyether ether ketone (PEEK), by copper coating via cold spray*.
[80] Kong K., Davies R.J., Young R.J., Eichhorn S.J., *Molecular and crystal deformation in poly (aryl ether ether ketone, fibers*, Macromolecules, **41**, 2008, p. 7519–7524.
[81] Johnson G.R., Cook W.H., *A constitutive model and data for metals subjected to large strains, high strain rates and high temperatures*, Proceedings of the 7th International Symposium on Ballistics, The Hague, The Netherlands, 1983, p. 541–547
[82] Assadi H., Kreye H., Gärtner F., Klassen T., *Cold spraying — a materials perspective*, Acta Mater., **116**, 2016, p. 382–407
[83] King P.C., Poole A.J., Horne S., de Nys R., Gulizia S., Jahedi M.Z., *Embedment of copper particles into polymers by cold spray*, Surf. Coat. Technol. 216 2013, 60-67. mposites, 2nd ed., William Andrew Publishing, Norwich, 2013, p. 189-714.
[84] King P.C., Poole A.J., Horne S., de Nys R., Gulizia S., Jahedi M.Z., *Embedment of copper particles into polymers by cold spray*, Surf. Coat. Technol., **216**, 2013, p. 60–67.
[85] Kong K., Davies R.J., Young R.J., Eichhorn S.J., *Molecular and crystal deformation in poly (aryl ether ether ketone, fibers*, Macromolecules, **41**, 2008, p. 7519–7524.
[86] Kong K., Davies R.J., Young R.J., Eichhorn S.J., *Molecular and crystal deformation in poly (aryl ether ether ketone, fibers*, Macromolecules, **41**, 2008, p. 7519–7524.

[87] Rija Nirina Raoelison, Libin Lalu Koithara, Sophie Costil, *Cold spray coating of PEEK surface by copper deposition: Interfacial adhesion at high deposition efficiency and bonding strength*, https://doi.org/10.1016/j.cirpj.2021.05.008
[88] Schmidt T., Gärtner F., Assadi H., Kreye H., *Development of a generalized parameter window for cold spray deposition*, Acta Mater., **54**, 3, 2006, p. 729–742.
[89] Fukumoto M., Mashiko M., Yamada M., Yamaguchi E., *Deposition behavior of copper fine particles onto flat substrate surface in cold spraying*, J. Therm. Spray Technol., **19**, 2010, p. 89–94.
[90] Meng F., Hu D., Gao Y., Yue S., Song J., *Cold-spray bonding mechanisms and deposition efficiency prediction for particle/substrate with distinct deformability*, Mater. Des., **109**, 2016, **p.** 503–510.
[91] Bae G., Xiong Y., Kumar S., Kang K., Lee C., *General aspects of interface bonding in kinetic sprayed coatings*, Acta Mater. 56, **17**, 2008, p. 4858–4868.
[92] Aleksandra Małachowska, Marcin Winnicki, Łukasz Konat, Tomasz Piwowarczyk, Lech Pawłowski, Andrzej Ambroziak, Mateusz Stachowicz, *Possibility of spraying of copper coatings on polyamide 6 with low pressure cold spray method*.
[94] Assadi H., Gärtner F., Stoltenhoff T., Kreye H., Acta Mater., **51**, 2003, p. 4379–4394.
[95] Grujicic M., Zhao C., DeRosset W., Helfritch D., Mater. Des., **25**, 2004, p. 681–688
[96] Hussain T., McCartney D.G., Shipway P.H., Zhang D., J. Therm. Spray Technol., **18**, 2009, p. 364–379.
[97] Ganesan A., Affi J., Yamada M., Fukumoto M., Surf. Coat. Technol., **207**, 2012, p. 262–269.
[98] Ganesan A., Yamada M., Fukumoto M., J. Therm. Spray Technol., **22**, 2013, p. 1275–1282
[99] Sudharshan Phani P., Srinivasa Rao D., Joshi S.V., Sundararajan G., J. Therm. Spray Technol., **16**, 2007, p. 425–434.
[100] Nigam S., Mahapatra S. S. & Patel S. K., *Effect of stand-off distance in thermally sprayed copper coating*.
[101] Sarikaya O., *Effect of some parameters on microstructure and hardness of alumina coatings prepared by the air plasma spraying process*, Surf Coat Technol., **190**, 2–3, 2005, p. 388–393.
[102] Wang Y, Li C, Ohmori A. *Influence of substrate roughness on the bonding mechanisms of high velocity oxyfuel sprayed coatings*, Thin Solid Films, **485**, 1, 2005, p. 141–147.
[103] Gonzalez R, McDonald A, Mertiny P., *Effect of flamesprayed Al-12Si coatings on the failure behaviour of pressurized fibre-reinforced composite tubes*, Polym Test, **32**, 8, 2013, p. 1522–1528.
[104] Liu A, Guo M, Zhao M, et al., *Arc sprayed erosionresistant coating for carbon fiber reinforced polymer matrix composite substrates*, Surf Coat Technol., 200, 2006, p. 3073–3077.
[105] Nourouzi S, Azizpour MJ, Salimijazi HR., *Parametric study of residual stresses in HVOF thermally spray*, http://dx.doi.org/10.1080/10426914.2014.921696
[106] Li D, Yang CL, *Acidic electroless copper deposition on aluminum-seeded ABS plastics*, Surf Coat Technol., **203**, 23, 2009, p. 3559–3568.
[107] Sushanta Kumar Sahoo1, Anshuman Kumar Sahu, Siba Sankar Mahapatra, *Environmental friendly electroless copper metallization on FDM build ABS parts*.
[108] Domenech SC, Lima E, Drago V, De Lima JC, Borges NG, Avila AOV, Soldi V., (2003, *Electroless plating of nickel–phosphorous on surface-modified poly (ethylene terephthalate, films*, Appl Surf Sci., **220**, 1, p. 238–250.
[109] Piotr Rytlewski, Bartłomiej Jagodzinski, Tomasz Karasiewicz, Piotr Augustyn, Daniel Kaczor, Rafał Malinowski, Krzysztof Szablinski, Marcin Mazurkiewicz, Krzysztof Moraczewski, *Copper Filled Poly(Acrylonitrile-co-Butadiene-co-Styrene, Composites for Laser-Assisted Selective Metallization*, http://dx.doi.org/10.3390/ma13102224
[110]. Blom H., Yeh R., Wojnarowski R., Ling M., *Detection of degradation of ABS materials via DSC*, Thermochim., Acta, **442**, 2006, p. 64–66.
[111]. Bair H.E., Boyle D.J., Kelleher P.G., *The Effects of Light and Heat on the Rubber Content and Impact Strength of Acrylonitrile-Butadiene-Styrene*, Polym. Eng. Sci., **20**, 1980, p. 995–1001.
[112]. Suzuki M., Wilkie C., *The thermal degradation of acrylonitrile-butadiene-styrene terpolymer as studied by TGA/FTIR*, Polym. Degrad. Stab., **47**, 1995, p.217–221.
[113]. Ghaemy M., Scott G., *Photo- and thermal oxidation of ABS: Correlation of loss of impact strength with degradation of the rubber component*, Polym. Degrad. Stab., **3**, 1981, p. 233–242.

[114]. Wolkowicz M.D., Gagga S.K., *Effect of thermal aging on impact strength acrylonitrile-butadiene-styrene (ABS) terpolymer*,
http://dx.doi.org/10.1002/0471238961.01021911211209.a01.pub2